Protrudin serves as an adaptor molecule that connects KIF5 and its cargoes in vesicular transport during process formation

Fumiko Matsuzaki, Michiko Shirane, Masaki Matsumoto, and Keiichi I. Nakayama
Department of Molecular and Cellular Biology, Medical Institute of Bioregulation, Kyushu University, 3-1-1 Maidashi, Higashi-ku, Fukuoka, Fukuoka 812-8582, Japan; CREST, Japan Science and Technology Corporation (JST), Kawaguchi, Saitama 332-0012, Japan

ABSTRACT **Neurons are highly polarized cells with long neurites. Vesicular transport is required for neurite extension. We recently identified protrudin as a key regulator of vesicular transport during neurite extension. Expression of protrudin in nonneuronal cells thus induces formation of neurite-like membrane protrusions. We adopted a proteomics approach to identify proteins that associate with protrudin. Among the protrudin-associated proteins, including many with a function related to intracellular trafficking, we focused on KIF5, a motor protein that mediates anterograde vesicular transport in neurons. A coimmunoprecipitation assay confirmed that endogenous protrudin and KIF5 interact in mouse brain. Overexpression of KIF5 induced the formation of membrane protrusions in HeLa cells, reminiscent of the effect of protrudin overexpression. Forced expression of both protrudin and KIF5 promoted protrusion extension in a synergistic manner, whereas depletion of either protein attenuated protrusion formation. Protrudin facilitated the interaction of KIF5 with Rab11, VAP-A and -B, Surf4, and RTN3, suggesting that protrudin serves as an adaptor protein and that the protrudin–KIF5 complex contributes to the transport of these proteins in neurons. Given that mutation of protrudin or KIF5 is a cause of human hereditary spastic paraplegia, the protrudin–KIF5 axis appears to be integral to neuronal function.**

Monitoring Editor
Xueliang Zhu
Chinese Academy of Sciences

Received: Jan 25, 2011
Revised: Sep 26, 2011
Accepted: Sep 28, 2011

INTRODUCTION

Neurons are highly polarized cells with long neurites that subserve their contribution to neural networks, with the neuronal surface area being as much as 10,000 times that of other cell types. A neuron-specific transport system for membrane-bound vesicles that contain lipids and proteins is thought to be required for the extension and maintenance of neurites and for various aspects of neuronal function. During the establishment of neuronal polarity, such vesicles are transported in a directional manner within the cell, supplying new materials to the growing processes and distributing different sets of molecules to distinct domains (Futerman and Banker, 1996). Once established, the unique structure and compartmentalized molecular composition of neurites must be maintained throughout neuronal life by selective sorting or transport of membranous compartments to particular domains (Tang, 2001).

Kinesin-1 (also known as conventional kinesin) is a molecular motor protein that plays key roles in the polarized transport system of neurons and in neuronal polarity (Ferreira *et al.*, 1992; Kimura *et al.*, 2005; Hirokawa *et al.*, 2009; Konishi and Setou, 2009). It moves unidirectionally over long distances toward the plus end of microtubules and thereby mediates anterograde transport of its cargoes from the cell body to synapses formed by neurites. Kinesin-1 binds a wide variety of neuronal cargoes required for the establishment and maintenance of axonal or somatodendritic domains (Goldstein *et al.*, 2008; Hirokawa *et al.*, 2009). It consists of a dimer of KIF5

This article was published online ahead of print in MBoC in Press (http://www.molbiolcell.org/cgi/doi/10.1091/mbc.E11-01-0068) on October 5, 2011.

Address correspondence to: Keiichi I. Nakayama (nakayak1@bioreg.kyushu-u.ac.jp).

Abbreviations used: AD-HSP, autosomal dominant, hereditary spastic paraplegia; ALS, amyotrophic lateral sclerosis; ANOVA, analysis of variance; APP, amyloid precursor protein; BSA, bovine serum albumin; EGFP, enhanced green fluorescent protein; FBS, fetal bovine serum; GAPDH, glyceraldehyde-3-phosphate dehydrogenase; GDP, guanosine diphosphate; GST, glutathione *S*-transferase; HA, hemagglutinin epitope; IB, immunoblot analysis; IF, identification frequency; IP, immunoprecipitation; KLC, kinesin light chain; LC–MS/MS, liquid chromatography and tandem mass spectrometry; mCherry, monomeric Cherry; mRFP, monomeric red fluorescent protein; Ni-NTA, nickel-nitrilotriacetic acid; NSF, *N*-ethylmaleimide-sensitive factor; PBS, phosphate-buffered saline; PMSF, phenylmethylsulfonyl fluoride; RNAi, RNA interference; RT, reverse transcription; RTN3, reticulon 3; shRNA, short hairpin RNA; siRNA, short interfering RNA; SNAP, soluble NSF attachment protein; Surf4, surfeit locus protein 4; VAP, vesicle-associated membrane protein–associated protein.

(kinesin heavy chain), which hydrolyzes ATP and uses the released energy to move along microtubules, as well as two regulatory kinesin light chains (KLCs; Hirokawa and Noda, 2008). KIF5 consists of an NH_2-terminal motor domain, a central coiled-coil stalk domain, and a COOH-terminal globular tail domain (Yang *et al.*, 1989). The tail of the kinesin molecule, encompassing the COOH-terminus of KIF5 and KLC, is the region most likely to mediate cargo binding (Goldstein, 2001; Hirokawa and Noda, 2008).

We recently identified protrudin as a key regulator of Rab11-dependent vesicular transport during neurite formation (Shirane and Nakayama, 2006). Rab11 regulates recycling pathways from endosomes to the plasma membrane (Stenmark, 2009) and is thought to contribute to the establishment of neuronal polarity through regulation of polarized vesicular transport. Protrudin contains an atypical Rab11-binding domain and promotes neurite formation through interaction with the guanosine diphosphate (GDP)-bound form of Rab11 (Shirane and Nakayama, 2006). The association of protrudin with Rab11 is promoted by protrudin phosphorylation, which results from extracellular signal–regulated kinase signaling triggered by nerve growth factor. Forced expression of protrudin in cultured cells, even in nonneuronal cells, induced localized membrane protrusion and the consequent formation of long processes, whereas down-regulation of protrudin by RNA interference (RNAi) induced membrane extension in all directions, resulting in inhibition of neurite formation.

The gene encoding ZFYVE27, a synonym of human protrudin (SPG33), was recently found to be mutated in a German family with an autosomal dominant form of hereditary spastic paraplegia (AD-HSP; Mannan *et al.*, 2006b). AD-HSP comprises a group of neurodegenerative disorders characterized by bilateral and slowly progressive spasticity of the legs that is associated with retrograde degeneration of axons in corticospinal tracts (Reid, 1997; Deluca *et al.*, 2004). It has been proposed that abnormal axonal transport of certain cargoes, particularly in the distal region of long axons underlies the disease process, as suggested by the finding that mutations in the gene for KIF5A, a neuron-specific isoform of KIF5 (SPG10), are also associated with HSP (Reid *et al.*, 2002; Goizet *et al.*, 2009). These various observations also suggest that protrudin plays a key role in polarized vesicular transport, not only during the establishment of neuronal polarity, but also during its maintenance. The precise mechanism by which protrudin regulates polarized vesicular transport has remained unclear.

With the use of proteomic screening, we have now identified KIF5A, KIF5B, and KIF5C as proteins that interact with protrudin. Furthermore, overexpression of KIF5 in HeLa cells induced the formation of membrane protrusions similar to those induced by protrudin overexpression. Both protrudin and KIF5 were shown to be required for such protrusion formation. Our results suggest that protrudin and KIF5 perform related functions in polarized vesicular transport. The genetic association of protrudin and KIF5 with a human neurodegenerative disease further suggests that the protrudin–KIF5 axis and its role in the polarized transport system are physiologically important for neuronal function.

RESULTS

Identification of protrudin-associated proteins by a proteomics approach

To investigate the physiological role of protrudin, we adopted a proteomics approach to identify proteins with which protrudin is physically associated in cells. Mouse protrudin tagged with hexahistidine (His_6) and the FLAG epitope in tandem at its NH_2-terminus was stably expressed in Neuro2A cells and then purified together with its associated proteins from cell lysates by dual-affinity chromatography with antibodies to FLAG (anti-FLAG) and with nickel-nitrilotriacetic acid (Ni-NTA) resin (Supplemental Figure S1). Proteins in the final eluate were fractionated by SDS–PAGE and stained with silver (Figure 1A). The stained gel was then sliced, the gel pieces were exposed to trypsin, and the generated peptides were subjected to liquid chromatography and tandem mass spectrometry (LC–MS/MS; Supplemental Table S1). We identified a total of 82 proteins that were present in all three replicates from cells overexpressing protrudin but which were not recovered from control cells (Table S2). Functional categorization of the protrudin-associated proteins with the PANTHER classification system revealed that a substantial proportion of these proteins (n = 21 or 26%) was related to intracellular protein traffic (Figure 1B), supporting the notion that protrudin plays a key role in vesicular transport. These latter proteins were subjected to semiquantitative analysis on the basis of the normalized identification frequency (IF) in each LC–MS/MS experiment (Figure 1C). Vesicle-associated membrane protein–associated protein A (VAP-A) and VAP-B, which we previously identified as protrudin-associated proteins (Saita *et al.*, 2009), were ranked first and third in the list. These results therefore justified our approach and revealed its high reproducibility. The protrudin-interacting proteins also included members of the KIF5 family, all of which are molecular motors that play key roles in trafficking of proteins or organelles in neurons.

Protrudin physiologically associates with KIF5 in mouse brain

To confirm the interaction between protrudin and KIF5 family members, we performed a coimmunoprecipitation assay. Immunoprecipitates were prepared with anti-FLAG from lysates of HEK293T cells transfected with expression vectors both for His_6-FLAG–tagged protrudin and for hemagglutinin epitope (HA)-tagged forms of mouse KIF5A, KIF5B, KIF5C, or KIF1Bα (known to transport some cargoes in neurons; used here as a negative control) lacking the head domain. The resulting precipitates were then subjected to immunoblot analysis (IB) with anti-HA and anti-FLAG (Figure 1D). All three isoforms of KIF5, but not KIF1Bα, were detected in the immunoprecipitates, with KIF5A being most efficiently coimmunoprecipitated with His_6-FLAG–protrudin.

Similar analysis was performed to detect the potential interaction between endogenous proteins. Immunoprecipitates from mouse brain extracts prepared with anti-protrudin were subjected to IB with anti-KIF5. Endogenous KIF5 was coimmunoprecipitated with endogenous protrudin (Figure 1E). Collectively, these results suggested that protrudin interacts with KIF5 in the brain under physiological conditions.

We next investigated which region of KIF5A is required for binding to protrudin by generating a series of HA-tagged deletion mutants of KIF5A and examining their ability to associate with His_6-FLAG–protrudin in a coimmunoprecipitation assay with HEK293T cells (Figure 2, A–D). Whereas full-length KIF5A and all three mutants that included the NH_2-terminal region of the stalk domain (amino acids 402–572) interacted with protrudin, all of the five mutants that lacked this region failed to do so, suggesting that the NH_2-terminal region of the stalk domain is necessary and sufficient for the interaction of KIF5A with protrudin.

We also determined the region of protrudin that is required for its binding to KIF5A (Figure 2, E–H). Whereas full-length protrudin and all six mutants that included the region containing the FFAT sequence, the coiled-coil domain, and the NH_2-terminal portion of the FYVE domain (amino acids 274–361) interacted with KIF5A(402–572), all six mutants that lacked this region failed to do

so, suggesting that the COOH-terminal region (amino acids 274–361) of protrudin is necessary and sufficient for its interaction with KIF5A.

To examine the direct interaction between KIF5A and protrudin in vitro, we performed a pulldown assay. Recombinant mutants of KIF5A tagged with glutathione *S*-transferase (GST) at their NH_2-termini were produced in bacteria and tested for their ability to bind to recombinant His_6-tagged protrudin produced in insect cells (Figures 3 and S2). Whereas KIF5A(402–572) bound to protrudin, KIF5A(1–401) and KIF5A(573–1027) did not, consistent with our observations in vivo. These results suggested the NH_2-terminal region of the stalk domain mediates the direct binding of KIF5A to protrudin.

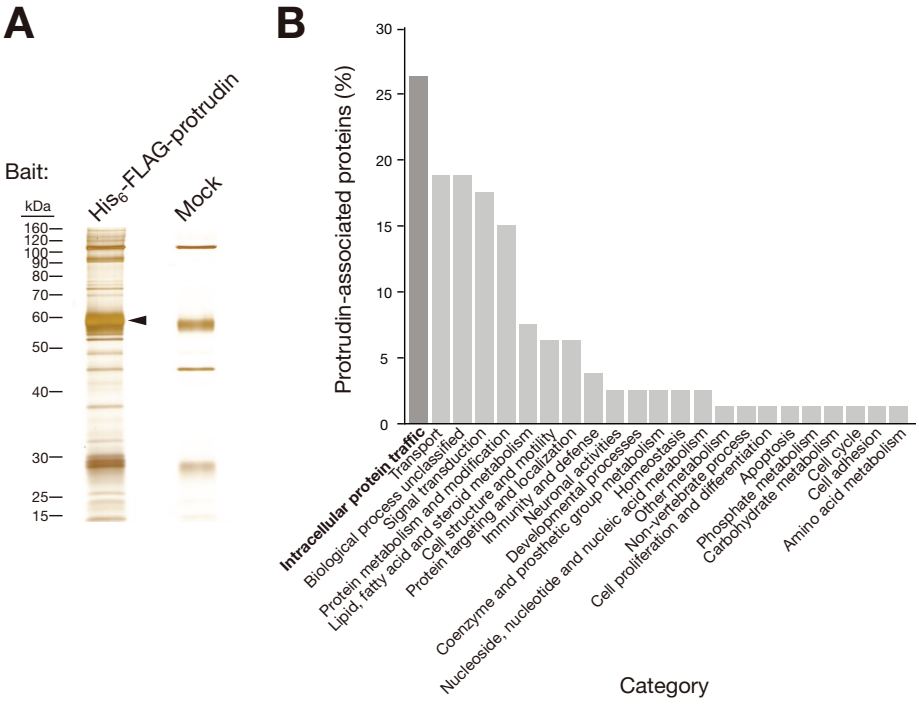

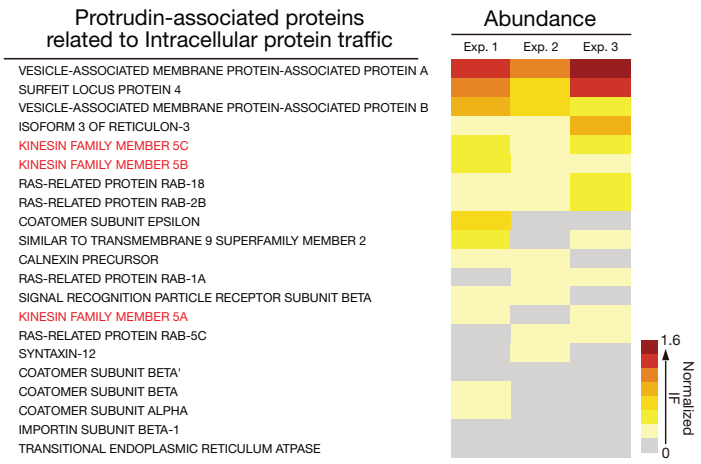

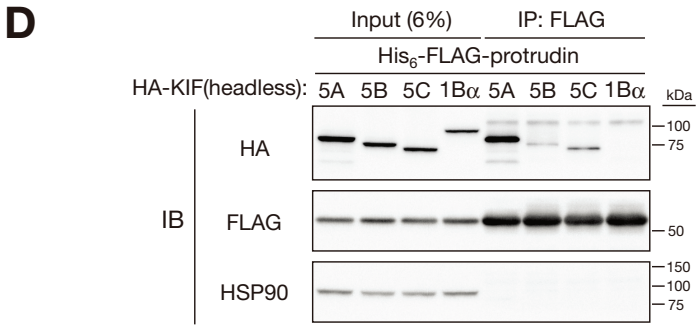

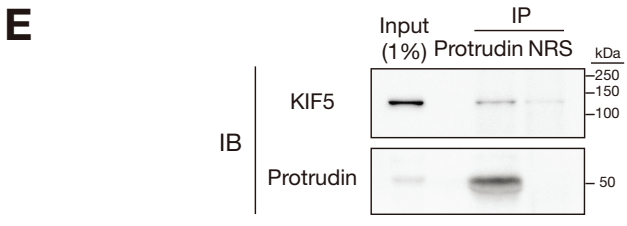

FIGURE 1: Identification of KIF5 family members as protrudin-associated proteins. (A) Neuro2A cells stably expressing His_6-FLAG–tagged mouse protrudin or infected with the corresponding empty virus (Mock) were lysed and subjected to dual-affinity chromatography with anti-FLAG and Ni-NTA agarose. The purified proteins were fractionated by SDS–PAGE and stained with silver. The arrowhead indicates the band corresponding to the bait protein. (B) The identified proteins that associated specifically with His_6-FLAG–protrudin were categorized according to their related gene ontology biological processes. The percentage contributions of each of the 23 functional categories to the total identified proteins are shown. (C) Proteins associated with intracellular protein traffic that were categorized in (B). The amount of each protein was estimated semiquantitatively on the basis of the normalized IF and is shown according to the indicated color scale in three independent experiments (Exp. 1–3). The proteins were ranked according to the average of the scores from the three experiments. (D) Extracts of HEK293T cells transiently transfected with expression vectors for His_6-FLAG–protrudin and for 2×HA-tagged headless forms of KIF5A, KIF5B, KIF5C, or KIF1Bα were subjected to IP with anti-FLAG. The resulting precipitates, as well as a portion (6% of the input for IP) of the cell extracts, were subjected to IB with anti-HA, anti-FLAG, or anti-HSP90 (loading control). (E) Mouse brain extract was subjected to IP with anti-protrudin or normal rabbit serum (NRS), and the resulting precipitates, as well as a portion (1% of the input for IP) of the tissue extract, were subjected to IB with anti-KIF5 and anti-protrudin.

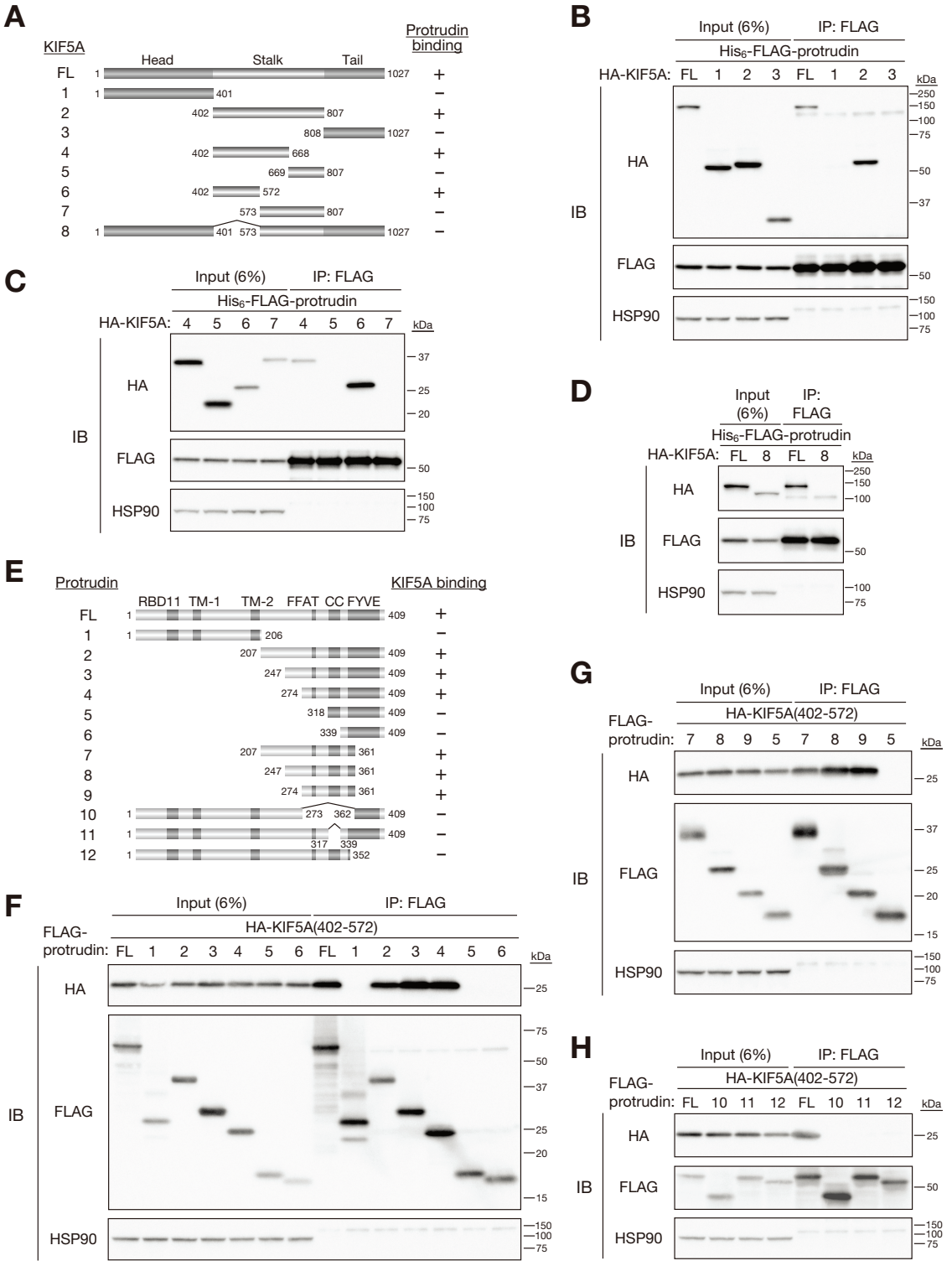

FIGURE 2: Delineation of the regions of KIF5A and protrudin responsible for their interaction. (A) Domain organization of mouse KIF5A and structure of deletion mutants thereof. A summary of the ability of the mutants to bind protrudin as determined in (B)–(D) is shown on the right. (B–D) Full-length (FL) KIF5A or its mutants shown in (A) fused at their NH_2-termini to the 2×HA tag were expressed in HEK293T cells together with His_6-FLAG–tagged mouse protrudin. Cell extracts were subjected to IP with anti-FLAG, and the resulting precipitates, as well as a portion (6% of the input for IP) of the cell extracts, were subjected to IB with anti-HA, anti-FLAG, or anti-HSP90. (E) Domain organization of human protrudin and structure of deletion mutants thereof. A summary of the ability of the mutants to bind KIF5A, as determined in (F)–(H), is shown on the right. (F–H) Full-length protrudin or its mutants shown in (E) fused at their NH_2-termini to the 3×FLAG tag were expressed in HEK293T cells together with 2×HA-tagged KIF5A(402–572). Cell extracts were subjected to IP with anti-FLAG, and the resulting precipitates, as well as a portion (6% of the input for IP) of the cell extracts, were subjected to IB with anti-HA, anti-FLAG, or anti-HSP90.

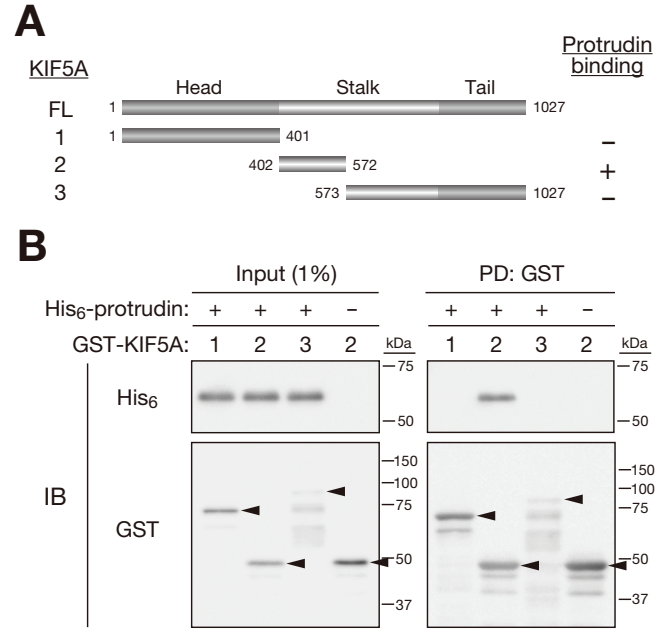

FIGURE 3: Protrudin directly associates with KIF5A. (A) Structure of mouse KIF5A mutants and a summary of their ability to bind to protrudin as determined in (B). (B) KIF5A mutants shown in (A) and fused at their NH_2-termini with GST were subjected to precipitation with glutathione-conjugated beads, and the beads were then incubated with His_6-tagged human protrudin. The bead-bound proteins (pulldown [PD]), as well as a portion (1%) of the protein input for precipitation, were subjected to IB with anti-His_6 or anti-GST. The arrowheads indicate bands corresponding to the GST-tagged KIF5A mutants.

Protrudin–KIF5 interaction is required for process formation in HeLa cells

Protrudin is necessary for neurite extension in neurons, and protrusion-forming activity is also apparent in transfected nonneuronal cells, such as HeLa cells overexpressing protrudin (Shirane and Nakayama, 2006; Saita *et al*., 2009). Although protrusion formation in HeLa cells might not be identical to neurite formation in neuronal cells, it likely reflects an activity of protrudin required for polarized vesicular transport that may be common to both HeLa and neuronal cells. We therefore adopted HeLa cells as an experimental system to estimate the activity of protrudin. To evaluate the role of KIF5 in the function of protrudin, we examined the effect of short hairpin RNA (shRNA)-mediated depletion of KIF5B on the protrusion-forming activity of protrudin in HeLa cells, given that among the KIF5 isoforms only KIF5B was found to be expressed in these cells (Figures 4A and S3A). Depletion of KIF5B resulted in marked inhibition of the protrusion-forming activity of protrudin, even though the expression level of protrudin was not affected (Figures 4, B and C, and S3B). We also examined the effect of expression of HA-tagged KIF5A(402–572), which associated with the KIF5A-binding region of protrudin and inhibited the interaction between KIF5A and protrudin (Figure S3D). The inhibition of the interaction between protrudin and KIF5 resulted in marked inhibition of the protrusion-forming activity of protrudin, even though the expression level of protrudin was not affected (Figures 4, D and E, and S3E). These results suggested KIF5 is required for the induction of protrusion formation by protrudin in HeLa cells.

We next examined the effect of KIF5A overexpression in HeLa cells. Cells overexpressing KIF5A exhibited marked changes in morphology, including the formation of membrane protrusions reminiscent of those observed in protrudin-overexpressing cells (Figure 5, A and B). In contrast, overexpression of KIF11, another member of the kinesin family, did not affect the morphology of HeLa cells (Figure S4A). KIF5A(T93N), a mutant with low ATPase activity that binds with high affinity to microtubules (Nakata and Hirokawa, 1995), also did not induce protrusion formation in HeLa cells (Figure S4B), suggesting the protrusion-forming activity of KIF5A depends on its ATPase activity.

Depletion of protrudin by RNAi resulted in marked inhibition of the protrusion-forming activity of KIF5A in HeLa cells, even though the expression level of KIF5A was not affected (Figures 5, C–E, and S3C). Furthermore, inhibition of the interaction between protrudin and KIF5 by expression of HA-tagged KIF5A(402–572) (Figure S3D) resulted in inhibition of the protrusion-forming activity of KIF5A, even though the expression level of KIF5A was not affected (Figures 5, F and G, and S3F). These results suggested that protrudin is necessary for the induction of protrusion formation by KIF5A. Collectively, our data indicated that the protrudin–KIF5 interaction promotes process formation.

We next investigated whether protrudin and KIF5 function synergistically during protrusion formation. Overexpression of both protrudin and KIF5A in HeLa cells indeed revealed an interaction between the two proteins and a synergistic effect on protrusion formation (Figures 5, H and I, and S3G). Synergism, rather than an additive effect, was confirmed by two-way analysis of variance (ANOVA; $p = 0.006$) and nonparallel lines in the interaction plot (Figure S5H) as well as by the Tukey-Kramer test ($p < 0.0001$; Figure 5I). These findings suggested protrudin and KIF5 perform related functions in protrusion formation.

Protrudin and KIF5 colocalize with Rab11b during protrusion formation

Protrudin and KIF5 are each necessary for the protrusion-formation activity of the other. We therefore next examined whether protrudin and KIF5A are colocalized at the site of protrusion formation. In HeLa cells expressing both enhanced green fluorescent protein (EGFP)-tagged KIF5A and monomeric red fluorescent protein (mRFP)-tagged protrudin, both fluorescence signals were most intense at the tip of the formed protrusions (Figure 6A). We also monitored protrusion formation by time-lapse video imaging and found that both fluorescence signals appeared to concentrate at the tip of the growing processes (Supplemental Movie S1 and Figure S5).

We next analyzed the localization of protrudin-mRFP and KIF5A-EGFP, as well as that of HA-tagged Rab11b, the GDP-bound form of which was previously shown to interact with protrudin (Shirane and Nakayama, 2006). Signals for protrudin, KIF5A, and Rab11b were colocalized at the tip of the formed protrusions and in the perinuclear region (Figure 6, B–D). We also analyzed the localization of protrudin-mRFP, KIF5A-EGFP, and HA-tagged Rab11b or Rab5b (which is localized to early endosomes and was examined as a negative control) in more detail by prefixation extraction of soluble proteins including KIF5, which is present in the cytosol in a folded conformation when not bound to cargoes (Coy *et al*., 1999; Cai *et al*., 2007), and Rab, which is present in the cytosol when complexed with a GDP dissociation inhibitor (Ullrich *et al*., 1993). Both protrudin and KIF5A signals were also colocalized with Rab11b under these conditions, but they did not colocalize with Rab5b (Figures 6, E–H, and Figure S6). These results suggested protrudin, KIF5, and Rab11b form a membrane-associated complex, consistent with the fact that protrudin has two putative transmembrane domains.

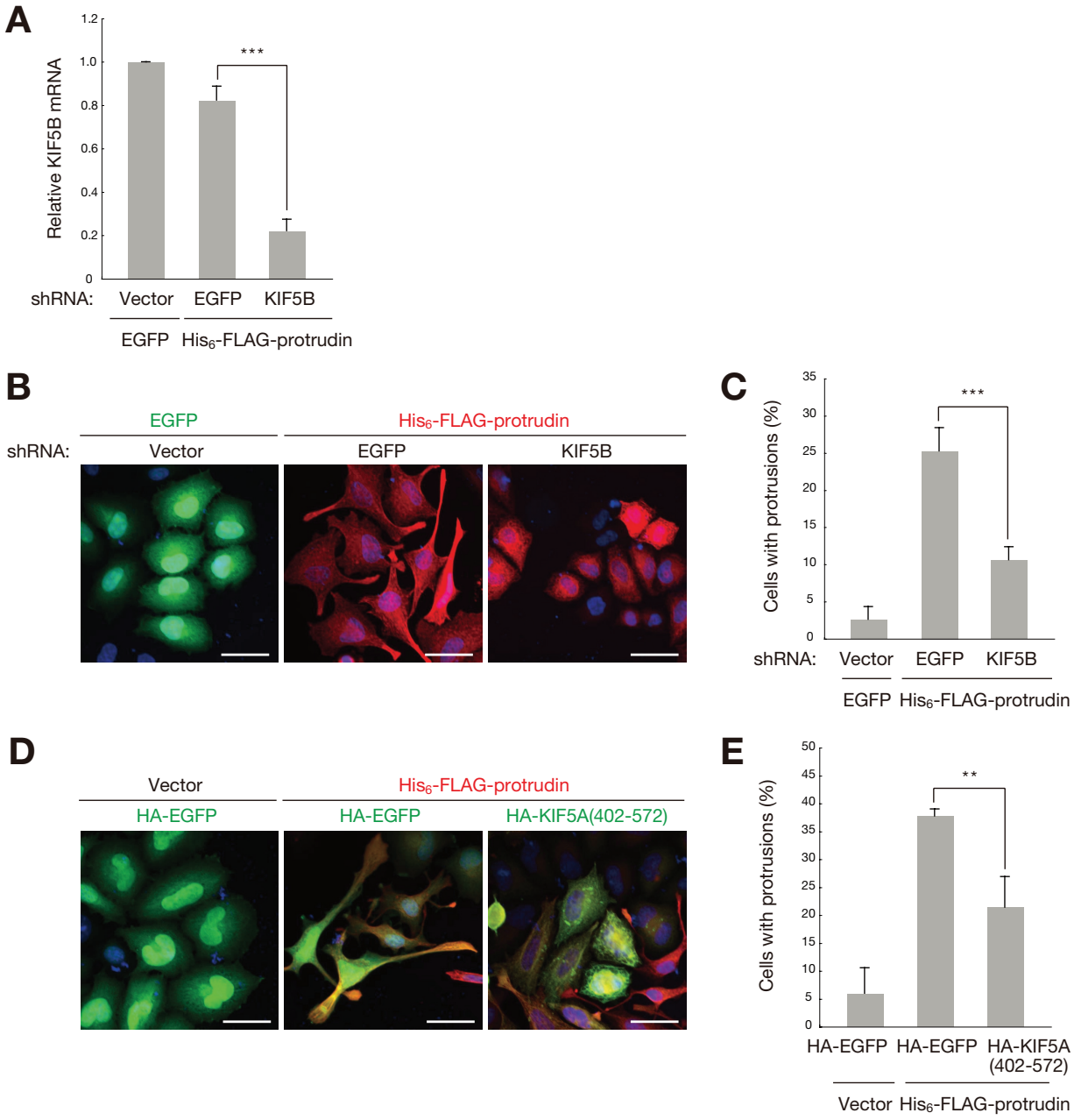

FIGURE 4: Protrusion formation induced by protrudin overexpression requires KIF5 in HeLa cells. (A) HeLa cells were transfected for 48 h with an expression vector for KIF5B shRNA (or for EGFP shRNA as a control] or with the empty vector, as well as with a vector for His_6-FLAG–tagged mouse protrudin (or EGFP), after which total RNA was extracted from the cells and subjected to RT and real-time PCR analysis of KIF5B mRNA. (B) HeLa cells treated as in (A) were subjected to immunofluorescence staining with anti-FLAG (red) or were monitored for direct fluorescence of EGFP (green). Nuclei were also stained with Hoechst 33258 (blue). Scale bars: 40 μm. (C) Quantitation of protrusion formation in cells treated as in (B). (D) HeLa cells transfected for 48 h with expression vectors for His_6-FLAG–tagged mouse protrudin and for 2×HA-tagged KIF5A(402–572) (or 2×HA-tagged EGFP) were subjected to immunofluorescence staining with anti-FLAG (red) and anti-HA (green). Nuclei were also stained with Hoechst 33258 (blue). Scale bars: 40 μm. (E) Quantitation of protrusion formation in cells treated as in (D). Quantitative data in (A), (C), and (E) are means ± SD from three independent experiments. **$p < 0.01$, ***$p < 0.001$ (one-way ANOVA, Tukey-Kramer test).

The protrudin–KIF5 complex colocalizes with Rab11, VAP-A and -B, Surf4, and RTN3 in neurites

Given that protrudin and KIF5 were shown to form a complex with Rab11b during protrusion formation in HeLa cells, we next examined whether protrudin, KIF5, and Rab11 are colocalized in rat pheochromocytoma PC12 cells expressing monomeric Cherry (mCherry)-tagged protrudin. The fluorescence signal for protrudin-mCherry colocalized with those for endogenous Rab11 and KIF5 in neurites (Figure 7A), suggesting protrudin, KIF5, and Rab11 form a complex in the neurites of neuronal cells.

Among the identified proteins that associate with protrudin and whose function is related to intracellular protein traffic (Figure 1, B and C, and Table S1), we also examined whether VAP-A and -B, surfeit locus protein 4 (Surf4), and reticulon 3 (RTN3) might be

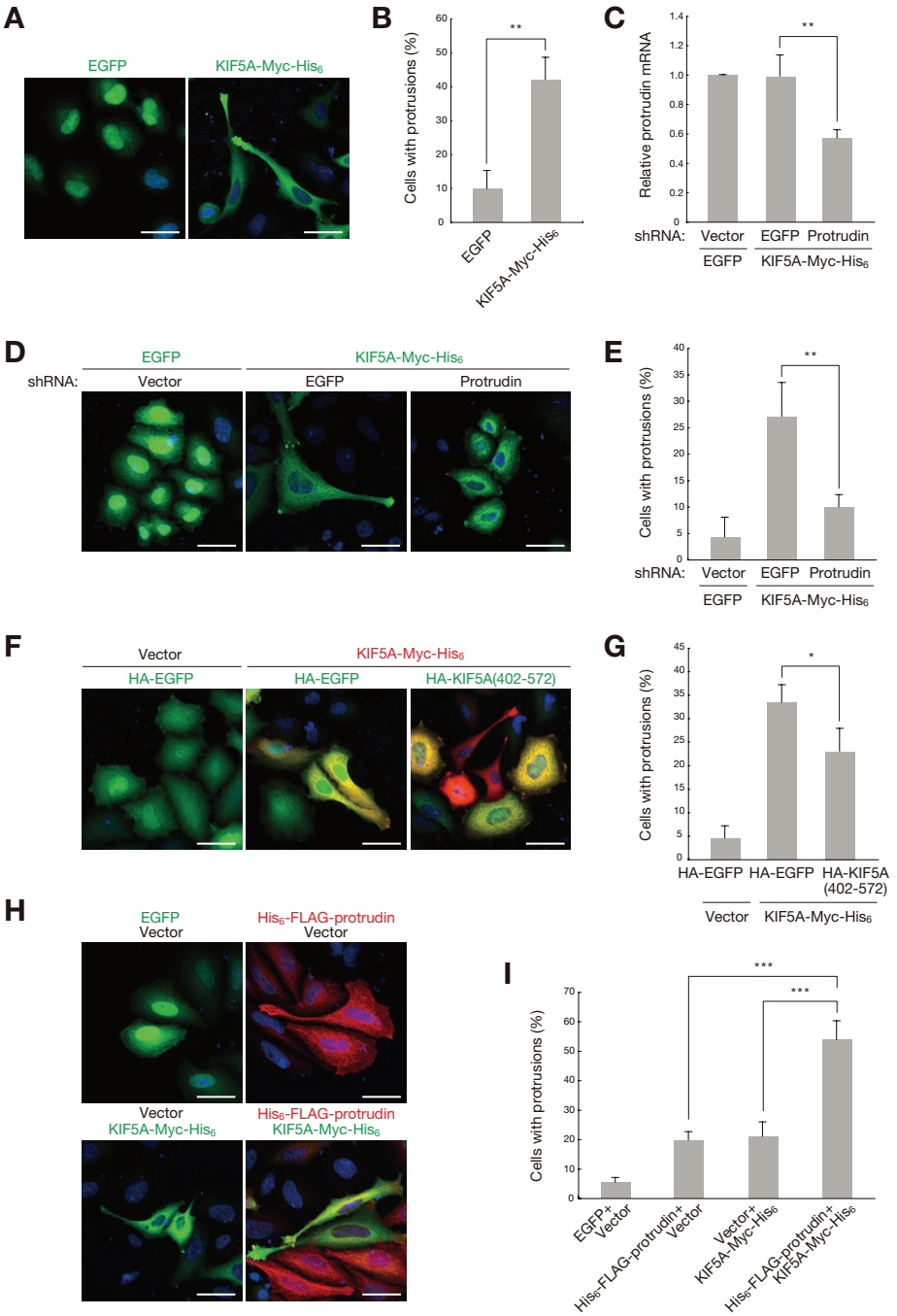

FIGURE 5: KIF5A overexpression induces protrusion formation in HeLa cells in a protrudin-dependent manner. (A) HeLa cells were transfected for 48 h with an expression vector for mouse KIF5A tagged with the Myc and His_6 epitopes (or for EGFP) and were then subjected to immunofluorescence staining with anti-Myc (green) or monitored for direct fluorescence of EGFP (green). Nuclei were also stained with Hoechst 33258 (blue). Scale bars: 40 μm. (B) Quantitation of protrusion formation in cells treated as in (A). (C) HeLa cells were transfected for 48 h with expression vectors for protrudin shRNA (or EGFP shRNA) and for KIF5A–Myc-His_6 (or EGFP), after which total RNA was extracted from the cells and subjected to RT and real-time PCR analysis of protrudin mRNA. (D) HeLa cells treated as in (C) were subjected to immunofluorescence staining with anti-Myc (green) or monitored for direct fluorescence of EGFP (green). Nuclei were also stained with Hoechst 33258 (blue). Scale bars: 40 μm. (E) Quantitation of protrusion formation in cells treated as in (D). (F) HeLa cells transfected for 48 h with expression vectors for KIF5A–Myc-His_6 and for 2×HA-tagged KIF5A(402–572) (or 2×HA-tagged EGFP) were stained with anti-Myc (red) and anti-HA (green). Nuclei were also stained with Hoechst 33258 (blue). Scale bars: 40 μm. (G) Quantitation of protrusion formation in cells treated as in (F). (H) HeLa cells transfected for 20 h with expression vectors for His_6-FLAG–tagged mouse protrudin (or EGFP) and for KIF5A–Myc-His_6, as indicated, were subjected to immunofluorescence staining with anti-FLAG (red) and anti-Myc (green) or were monitored for direct fluorescence of EGFP (green). Nuclei were also stained with Hoechst 33258 (blue). Scale bars: 40 μm. (I) Quantitation of process formation in cells treated as in (H). Quantitative data in (B), (C), (E), (G), and (I) are means ± SD from three independent experiments. *$p < 0.05$, **$p < 0.01$, ***$p < 0.0001$ (Student's *t* test in B; one-way ANOVA, Tukey-Kramer test in C, E, and G; two-way ANOVA, Tukey-Kramer test in I).

associated with the protrudin–KIF5 complex. In PC12 cells expressing HA-tagged VAP-A and protrudin-mCherry, both corresponding fluorescence signals colocalized with that for endogenous KIF5 in neurites (Figure 7B). Furthermore, in PC12 cells expressing protrudin-mCherry alone, the fluorescence signal colocalized with those for endogenous VAP-B and KIF5 in neurites (Figure 7C). Finally, HA-tagged Surf4 and HA-tagged RTN3 each colocalized with protrudin-mCherry and endogenous KIF5 in neurites (Figure 7, D and E). These results suggested that protrudin and KIF5 likely form complexes with VAP-A or -B, Surf4, or RTN3 in the neurites of neuronal cells.

Protrudin links Rab11b, VAP-A or -B, Surf4, or RTN3 to KIF5

Colocalization of protrudin, KIF5, and Rab11 in HeLa and PC12 cells suggested they form a complex with protrudin (Figures 6, B–H, and 7A). Our previous demonstration that protrudin interacts with the GDP-bound form of Rab11 (Shirane and Nakayama, 2006) and our present finding that protrudin directly associates with KIF5 (Figures 3 and S2) prompted us to examine whether protrudin might serve as an adaptor protein that links the GDP-bound form of Rab11 and KIF5. Coimmunoprecipitation experiments revealed that protrudin promoted the association of Rab11b(S25N), a mutant of Rab11b that preferentially binds to GDP, with an NH_2-terminal fragment (amino acids 1–572) of KIF5A [KIF5A(N)], whereas Rab11b(Q70L), a mutant of Rab11b that selectively binds to GTP and does not interact with protrudin (Figures 8A and S7, A and B; Shirane and Nakayama, 2006), did not associate with KIF5A(N) (Figure 8B). Furthermore, protrudin(ΔCC), a mutant of protrudin that lacks amino acids 324–344 and does not bind to KIF5A(N), did not promote the binding of Rab11b(S25N) to KIF5A(N) (Figure 8C). These results suggested protrudin serves as an adaptor protein that links the GDP-bound form of Rab11 to KIF5.

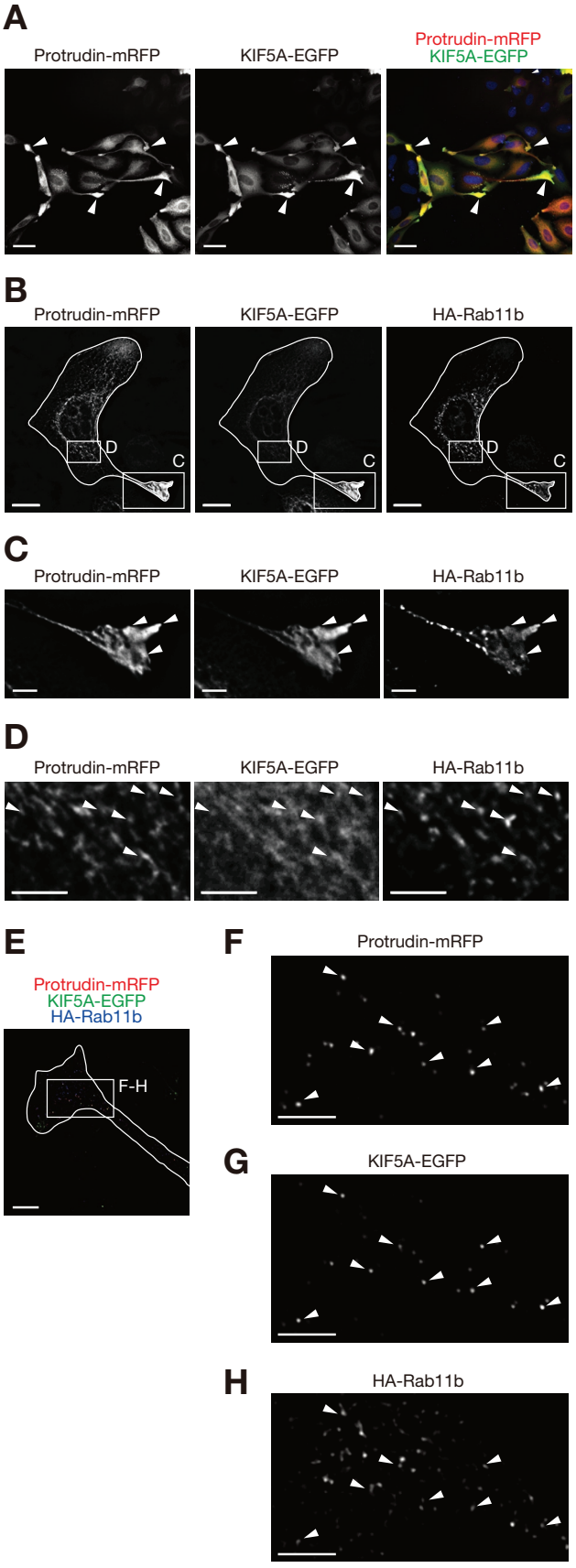

FIGURE 6: Protrudin and KIF5A colocalize with Rab11b during protrusion formation in HeLa cells. (A) HeLa cells expressing protrudin-mRFP and KIF5A-EGFP were fixed and monitored for direct fluorescence of mRFP (red) and EGFP (green) by deconvolution microscopy. Nuclei were stained with Hoechst 33258 (blue). Arrowheads indicate tips of protrusions at which protrudin and KIF5A colocalized. Scale bars: 40 μm. (B) HeLa cells expressing protrudin-mRFP, KIF5A-EGFP, and HA-tagged Rab11b were subjected to immunostaining with anti-HA and monitored for direct fluorescence of mRFP and EGFP by deconvolution microscopy. Deconvoluted images are shown, with the cell boundary outlined in white. Scale bars: 15 μm. (C and D) Enlarged images of the boxed area in (B) showing protrudin-mRFP, KIF5A-EGFP, and HA-Rab11b fluorescence signals. Arrowheads indicate colocalization of protrudin, KIF5A, and Rab11b. Scale bars: 5 μm. (E) HeLa cells expressing protrudin-mRFP (red), KIF5A-EGFP (green), and HA-tagged Rab11b were extracted with 0.1% Triton X-100 before fixation for immunostaining with anti-HA (blue). A deconvoluted image of the site of protrusion formation is shown, with the cell boundary outlined in white. Scale bar: 10 μm. (F to H) Enlarged images of the boxed area in (E) showing protrudin-mRFP, KIF5A-EGFP, and HA-Rab11b fluorescence signals, respectively. Arrowheads indicate colocalization of protrudin, KIF5A, and Rab11b. Scale bars: 5 μm.

We compared the abilities of Rab11a and Rab11b to bind to protrudin in coimmunoprecipitation experiments, finding that protrudin associated with GDP-Rab11a and GDP-Rab11b to similar extents (Figure S7C). We also examined the effects of short interfering RNA (siRNA)-mediated depletion of Rab11a or Rab11b on protrusion formation in HeLa cells. The siRNAs targeted to Rab11a or Rab11b mRNAs specifically and completely depleted the corresponding proteins (Figure S8A). Depletion of Rab11a or Rab11b by RNAi had no effect on protrusion formation induced by overexpression of protrudin (Figure S8, B–F) or of KIF5A (Figure S9) in HeLa cells. These results suggested Rab11a and Rab11b are functionally redundant in protrusion formation.

We next examined whether protrudin links VAP-A or -B, Surf4, or RTN3 to KIF5. Coimmunoprecipitation experiments revealed that protrudin promoted the binding of VAP-A or -B to KIF5A(N), whereas neither protrudin(ΔCC), which does not bind to KIF5A, nor the VAP-A(ΔTM) mutant, which does not interact with protrudin (Saita *et al.*, 2009), was able to substitute for the corresponding wild-type proteins in this regard (Figure 9A). We also confirmed the binding of Surf4 and protrudin in a coimmunoprecipitation assay (Figure 9B). Similar to the case of VAP-A and -B, protrudin promoted the binding of Surf4 to KIF5A(N), whereas protrudin(ΔCC) did not (Figure 9C). Coimmunoprecipitation experiments also revealed that protrudin interacted with RTN3 (Figure 9D) and promoted the binding of the latter to KIF5A(N) (Figure 9E).

We previously showed that protrudin directly associates with VAP-A in vitro (Saita *et al.*, 2009). A similar pulldown assay in vitro revealed the direct interaction of protrudin with VAP-B (Figure S10, A and B) and with RTN3 (Figure S10, C–E). Whereas wild-type VAP-B directly bound to protrudin in vitro, VAP-B(125–196)—a mutant corresponding to VAP-A(132–201), which does not bind to protrudin (Saita *et al.*, 2009)—failed to bind to protrudin (Figure S10B), suggesting the interaction between protrudin and VAP-B is specific. Similarly, whereas recombinant GST-RTN3 bound to protrudin, GST alone did not (Figure S10E). These results suggested protrudin directly associates with VAP-A and -B and RTN3. We were not able to express recombinant Surf4 in bacteria and so were not able to perform a corresponding pulldown assay.

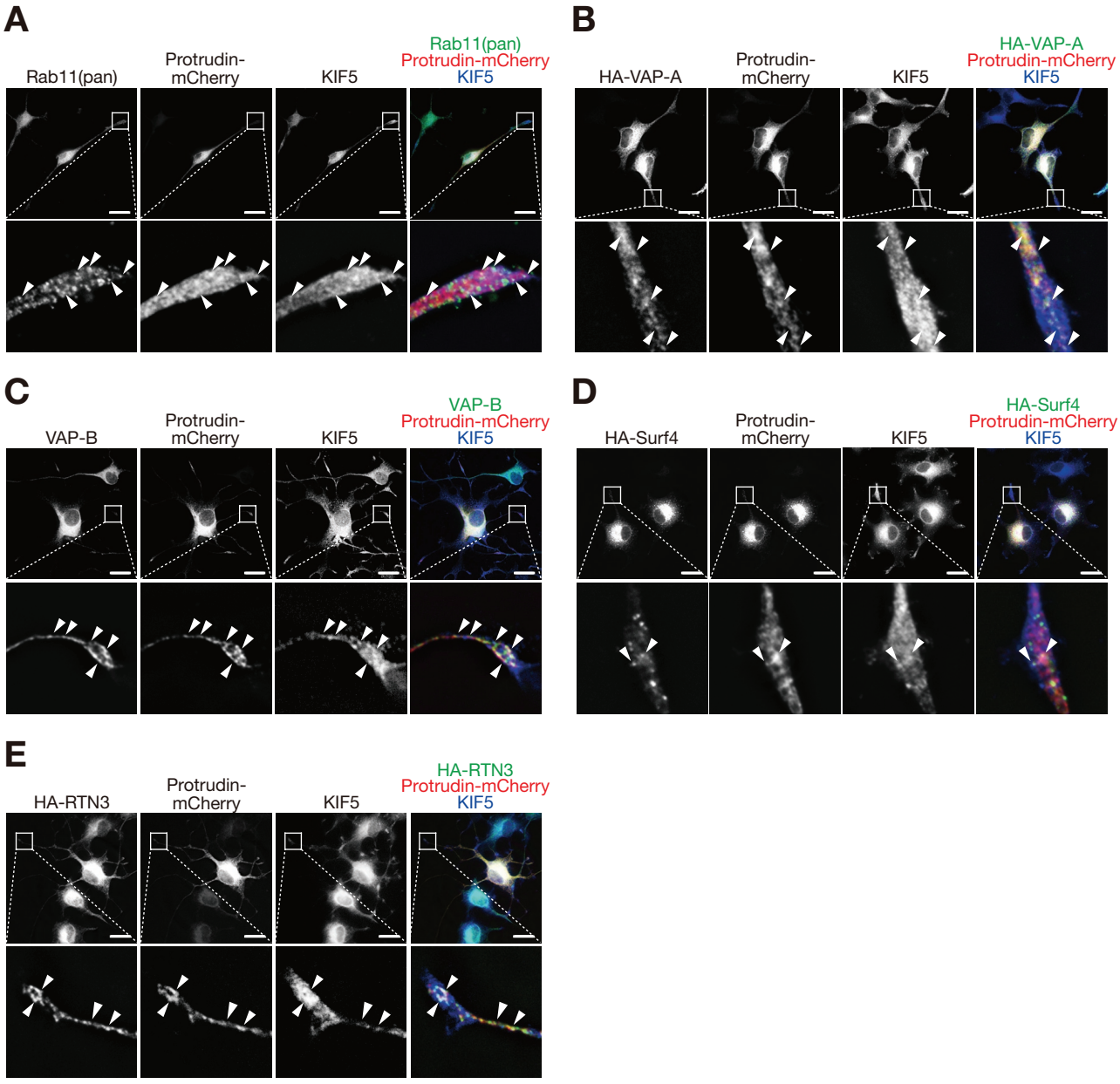

FIGURE 7: Protrudin and KIF5 colocalize with Rab11, VAP-A and -B, Surf4, and RTN3 in PC12 cells. (A) PC12 cells expressing protrudin-mCherry were subjected to immunofluorescence staining with anti-Rab11(pan) (green) and anti-KIF5 (blue) and were monitored for direct fluorescence of mCherry (red) by deconvolution microscopy. Deconvoluted images are shown, with the boxed areas in the top panels presented at higher magnification in the bottom panels. Arrowheads indicate colocalization of protrudin-mCherry, Rab11, and KIF5. Scale bars: 15 μm. (B) PC12 cells expressing protrudin-mCherry and HA–VAP-A were subjected to immunostaining with anti-HA (green) and anti-KIF5 (blue) and were monitored for direct fluorescence of mCherry (red) by deconvolution microscopy. Deconvoluted images are shown, with the boxed areas in the top panels presented at higher magnification in the bottom panels. Arrowheads indicate colocalization of protrudin-mCherry, HA–VAP-A, and KIF5. Scale bars: 15 μm. (C) PC12 cells expressing protrudin-mCherry were subjected to immunostaining with anti–VAP-B (green) and anti-KIF5 (blue) and were monitored for direct fluorescence of mCherry (red) by deconvolution microscopy. Deconvoluted images are shown, with the boxed areas in the top panels presented at higher magnification in the bottom panels. Arrowheads indicate colocalization of protrudin-mCherry, VAP-B, and KIF5. Scale bars: 15 μm. (D) PC12 cells expressing protrudin-mCherry and HA-Surf4 were subjected to immunostaining with anti-HA (green) and anti-KIF5 (blue) and were monitored for direct fluorescence of mCherry (red) by deconvolution microscopy. Deconvoluted images are shown, with the boxed areas in the top panels presented at higher magnification in the bottom panels. Arrowheads indicate colocalization of protrudin-mCherry, HA-Surf4, and KIF5. Scale bars: 15 μm. (E) PC12 cells expressing protrudin-mCherry and HA-RTN3 were subjected to immunostaining with anti-HA (green) and anti-KIF5 (blue) and were monitored for direct fluorescence of mCherry (red) by deconvolution microscopy. Deconvoluted images are shown, with the boxed areas in the top panels presented at higher magnification in the bottom panels. Arrowheads indicate colocalization of protrudin-mCherry, HA-RTN3, and KIF5. Scale bars: 15 μm.

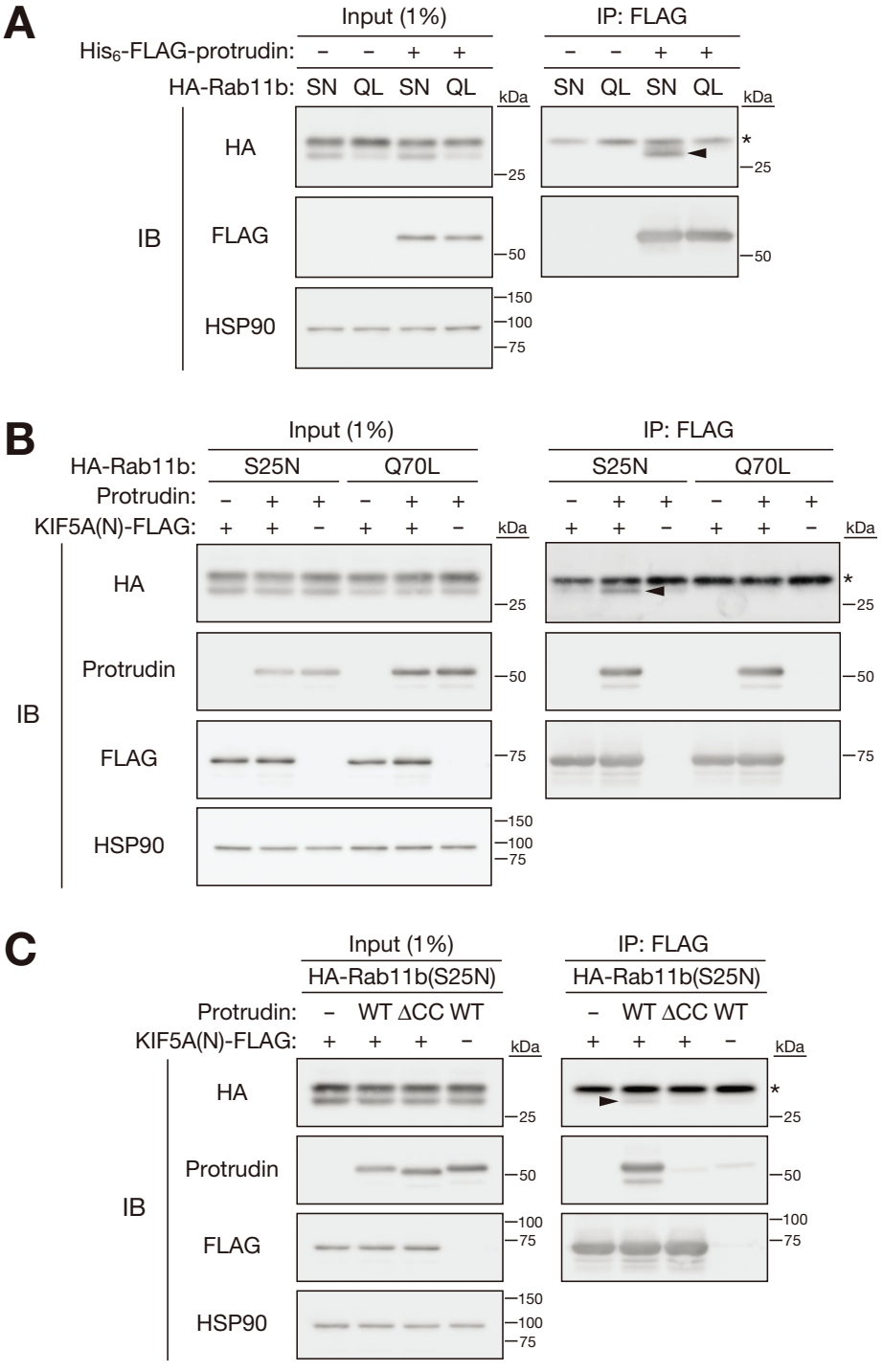

FIGURE 8: Protrudin links the GDP-bound form of Rab11b to KIF5A. (A) Extracts of HEK293T cells transiently transfected with expression vectors for His_6-FLAG–tagged mouse protrudin and for 2×HA-tagged S25N or Q70L mutants of human Rab11b were subjected to IP with anti-FLAG. The resulting precipitates, as well as a portion (1% of the input for IP) of the cell extracts, were subjected to IB with anti-HA, anti-FLAG, or anti-HSP90. The arrowhead indicates a band corresponding to 2×HA-tagged Rab11b(S25N) that coprecipitated with His_6-FLAG–protrudin, whereas the asterisk indicates nonspecific binding to beads. (B) Extracts of HEK293T cells transiently transfected with expression vectors for mouse protrudin, for 2×HA-tagged S25N or Q70L mutants of Rab11b, and for a FLAG-tagged NH_2-terminal fragment of mouse KIF5A (KIF5A(N), residues 1–572) were subjected to IP with anti-FLAG. The resulting precipitates, as well as a portion (1% of the input for IP) of the cell extracts, were subjected to IB with anti-HA, anti-protrudin, anti-FLAG, or anti-HSP90. The arrowhead indicates a band corresponding to 2×HA-tagged Rab11b(S25N) that coprecipitated with FLAG-tagged KIF5A(N), whereas the asterisk indicates nonspecific binding to beads. (C) Extracts of HEK293T cells transiently transfected with expression vectors for wild-type (WT) or ΔCC mutant (Δ324–344) forms of mouse protrudin, for 2×HA-tagged Rab11b(S25N), and for FLAG-tagged KIF5A(N) were subjected to IP with anti-FLAG. The resulting precipitates, as well as a portion (1% of the input for IP) of the cell extracts, were subjected to IB with anti-HA, anti-protrudin, anti-FLAG, or anti-HSP90. The arrowhead indicates a band corresponding to 2×HA-tagged Rab11b(S25N) that coprecipitated with FLAG-tagged KIF5A(N), whereas the asterisk indicates nonspecific binding to beads.

Rab11, VAP-A and -B, Surf4, and RTN3 are transported with protrudin–KIF5 from the soma to neurites in neuronal cells

We next investigated whether the protrudin–KIF5 complex is required for transport of Rab11 in neuronal cells. Inhibition of the interaction between protrudin and KIF5 by expression of mRFP-tagged KIF5A(402–572) in mouse cortical neurons resulted in the loss of protrudin-EGFP from neurites and its accumulation in the soma (Figure 10, A and B). The accumulated protrudin-EGFP colocalized to a large extent with mRFP-KIF5A(402–572), suggesting that protrudin that interacted with KIF5A(402–572) was not transported from the soma to neurites. We also found that more endogenous Rab11 was present in the soma of neurons expressing mRFP-KIF5A(402–572) and His_6-FLAG–protrudin than in that of neurons not expressing these proteins (Figure 10C). Furthermore, the accumulated Rab11 was highly colocalized with His_6-FLAG–protrudin and mRFP-KIF5A(402–572) (Figure 10C). Expression of mRFP-KIF5A(402–572) did not affect the localization of the Golgi apparatus as revealed by GM130 immunofluorescence (Figure 10D).

We also examined whether the protrudin–KIF5 complex is required for transport of VAP-A and -B, Surf4, and RTN3 in neuronal cells. In mouse cortical neurons expressing HA–VAP-A and His_6-FLAG–protrudin, VAP-A was localized along neurites with protrudin (Figure 11A). Inhibition of the interaction between protrudin and KIF5 by expression of mRFP-KIF5A(402–572), which competes with endogenous KIF5 for binding to protrudin, resulted in attenuation of normal vesicular transport of VAP-A to neurites and its consequent accumulation in the soma (Figure 11B). Similarly, VAP-B (Figure 11, C and D), Surf4 (Figure 11, E and F), and RTN3 (Figure 11, G and H) were localized along neurites with protrudin in a manner sensitive to the expression of KIF5A(402–572). These results suggested the protrudin–KIF5 complex is associated with potential cargoes, such as

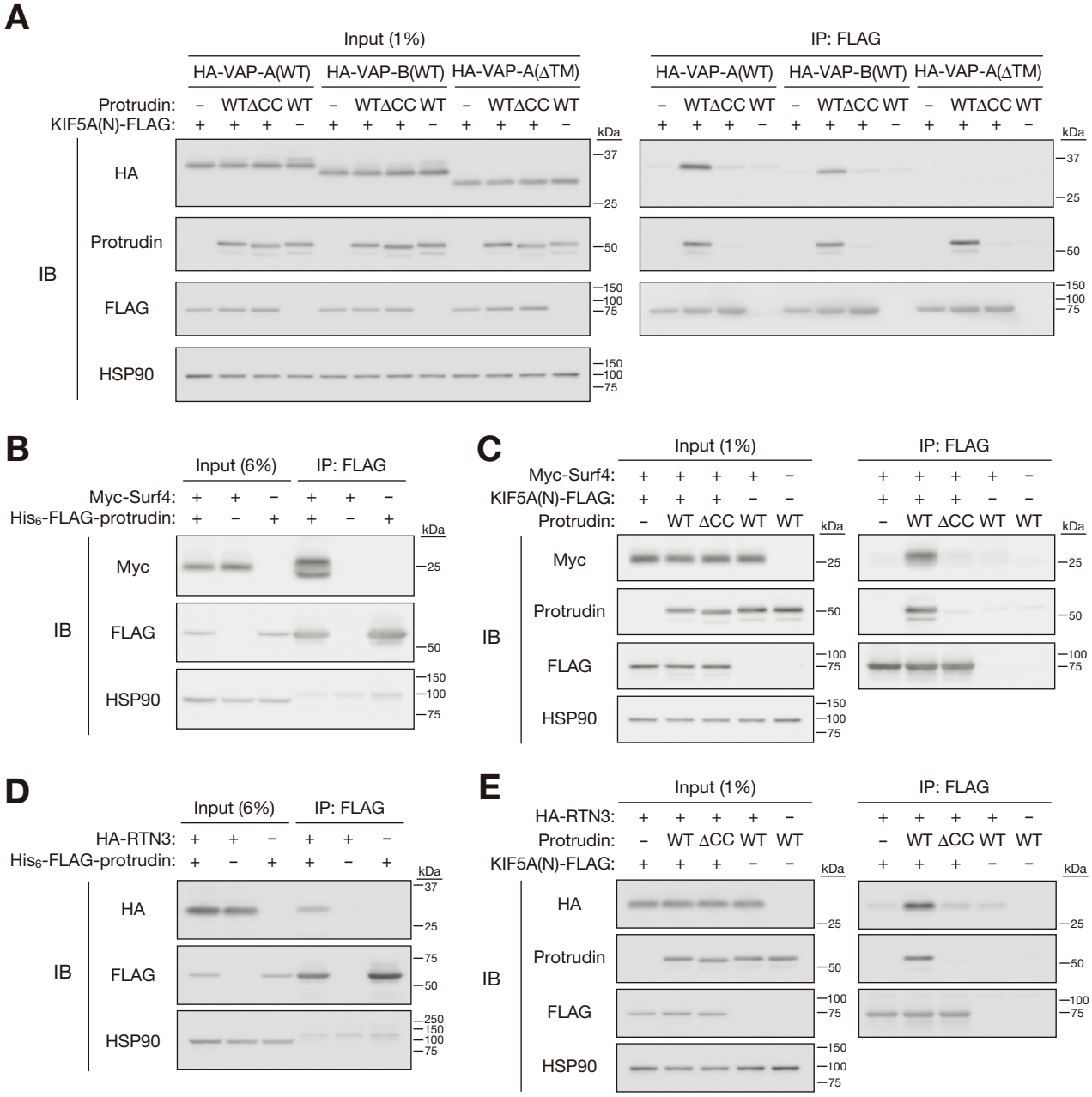

FIGURE 9: Protrudin links VAP-A or -B, Surf4, or RTN3 to KIF5A. (A) Extracts of HEK293T cells transiently transfected with expression vectors for 2×HA-tagged wild-type (WT) or ΔTM mutant (Δ228–249) forms of human VAP-A or WT human VAP-B, for protrudin (WT or ΔCC mutant), and for FLAG–tagged KIF5A(N) were subjected to IP with anti-FLAG. The resulting precipitates, as well as a portion (1% of the input for IP) of the cell extracts, were subjected to IB with anti-HA, anti-protrudin, anti-FLAG, or anti-HSP90. (B) Extracts of HEK293T cells transfected with expression vectors for His_6-FLAG–tagged protrudin and for 2×Myc-tagged mouse Surf4 were subjected to IP with anti-FLAG. The resulting precipitates, as well as a portion (6% of the input for IP) of the cell extracts, were subjected to IB with anti-Myc, anti-FLAG, or anti-HSP90. (C) Extracts of HEK293T cells transiently transfected with expression vectors for 2×Myc-tagged Surf4, for protrudin (WT or ΔCC mutant), and for FLAG-tagged KIF5A(N) were subjected to IP with anti-FLAG. The resulting precipitates, as well as a portion (1% of the input for IP) of the cell extracts, were subjected to IB with anti-Myc, anti-protrudin, anti-FLAG, or anti-HSP90. (D) Extracts of HEK293T cells transiently transfected with expression vectors for His_6-FLAG–tagged protrudin and for 2×HA-tagged human RTN3 were subjected to IP with anti-FLAG. The resulting precipitates, as well as a portion (6% of the input for IP) of the cell extracts, were subjected to IB with anti-HA, anti-FLAG, or anti-HSP90. (E) Extracts of HEK293T cells transiently transfected with expression vectors for protrudin (WT or ΔCC), for 2×HA-tagged RTN3, and for FLAG-tagged KIF5A(N) were subjected to IP with anti-FLAG. The resulting precipitates, as well as a portion (1% of the input for IP) of the cell extracts, were subjected to IB with anti-HA, anti-protrudin, anti-FLAG, or anti-HSP90.

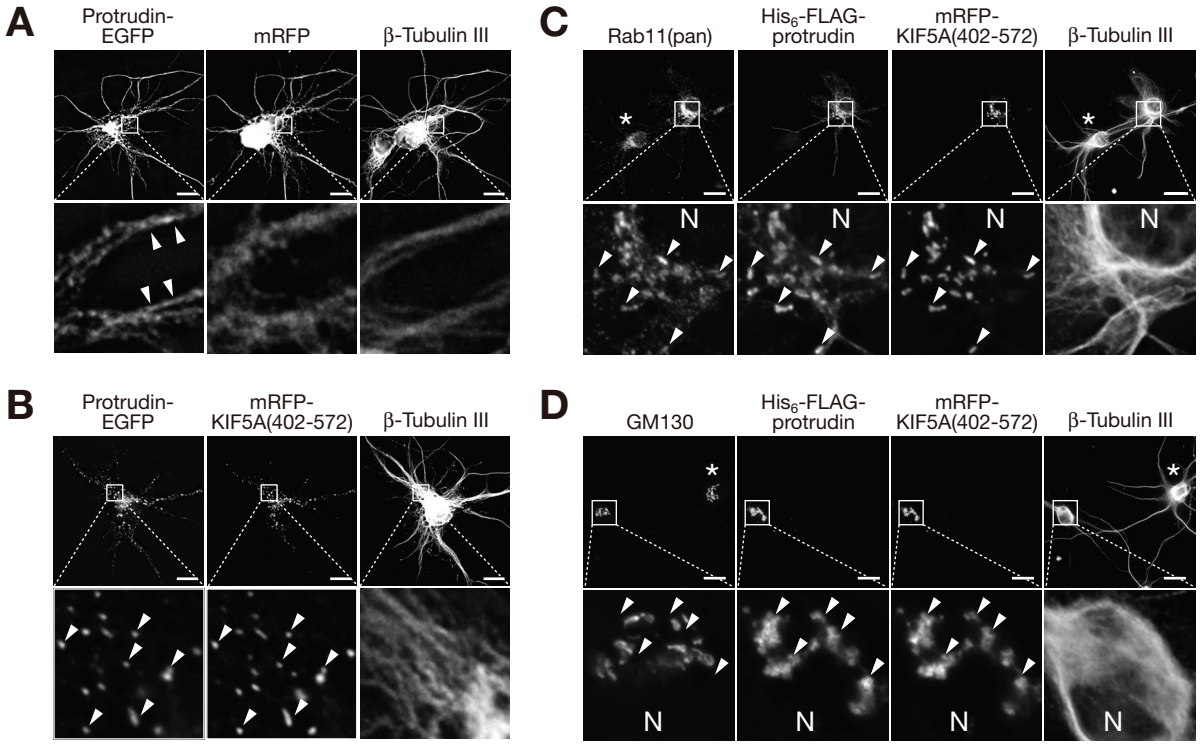

FIGURE 10: Protrudin accumulates with Rab11 in the soma of mouse cortical neurons in response to inhibition of its association with KIF5. (A) Mouse cortical neurons expressing protrudin-EGFP and mRFP were subjected to immunofluorescence staining with anti–β-tubulin III and monitored for direct fluorescence of EGFP and mRFP. Deconvoluted images are shown, with the boxed areas in the top panels presented at higher magnification in the bottom panels. Arrowheads indicate protrudin-EGFP signals along neurites. Scale bars: 5 μm. (B) Mouse cortical neurons expressing protrudin-EGFP and mRFP-KIF5A(402–572) were subjected to immunofluorescence staining with anti–β-tubulin III and monitored for direct fluorescence of EGFP and mRFP. Deconvoluted images are shown, with the boxed areas of the top panels presented at higher magnification in the bottom panels. Arrowheads indicate accumulation of protrudin–EGFP with mRFP-KIF5A(402–572) in the soma. Scale bars: 5 μm. (C) Mouse cortical neurons expressing mRFP-KIF5A(402–572) and His_6-FLAG–protrudin were subjected to immunofluorescence staining with anti-Rab11, anti-FLAG, and anti–β-tubulin III and were monitored for direct fluorescence of mRFP. Deconvoluted images are shown, with the boxed areas of the top panels presented at higher magnification in the bottom panels. The position of the nucleus is indicated by N. The asterisks indicate a neuron not expressing His_6-FLAG–protrudin or mRFP-KIF5A(402–572), whereas the arrowheads indicate colocalization of mRFP-KIF5A(402–572), His_6-FLAG–protrudin, and Rab11 in the soma. Scale bars: 15 μm. (D) Mouse cortical neurons expressing mRFP-KIF5A(402–572) and His_6-FLAG–protrudin were subjected to immunofluorescence staining with anti-GM130, anti-FLAG, and anti–β-tubulin III and were monitored for direct fluorescence of mRFP. Deconvoluted images are shown, with the boxed areas of the top panels presented at higher magnification in the bottom panels. The position of the nucleus is indicated by N. The asterisks indicate a neuron not expressing His_6-FLAG–protrudin or mRFP-KIF5A(402–572), whereas the arrowheads indicate colocalization of mRFP-KIF5A(402–572) and His_6-FLAG–protrudin, but not GM130. Scale bars: 15 μm.

Rab11, VAP-A and -B, Surf4, and RTN3 in neurites, and these cargoes are anchored to KIF5 through protrudin for vesicular transport from the soma to neurites.

DISCUSSION

Neuronal cells require motor proteins to ensure the localization of a wide variety of membrane proteins to the appropriate cellular domains; this allows the neuronal cells to establish and maintain their polarity. KIF5 is responsible for such proper distribution of a large number of cargo proteins associated with various types of intracellular vesicles (Hirokawa *et al.*, 2009). The docking of motor proteins to their cargoes via adaptor proteins is thought to be an important mechanism for achieving cargo selectivity and spatiotemporal control of cargo transport (Hirokawa *et al.*, 2009). Major adaptor proteins for KIF5 include KLCs (Gyoeva *et al.*, 2004). KLCs associate with scaffold proteins, such as c-Jun NH_2-terminal kinase–interacting proteins (JIP1 to -3) and CRMP2, which in turn interact with cargoes and link them to KIF5 (Hirokawa *et al.*, 2009). In other instances, KIF5 directly binds in a KLC-independent manner to adaptor proteins, such as GRIP1 (Setou *et al.*, 2002), the Milton–Miro complex (Glater *et al.*, 2006), syntabulin (Su *et al.*, 2004), and RanBP2 (Cho *et al.*, 2007). However, only a limited number of adaptor proteins has been shown to mediate the docking of a large number of cargo proteins to KIF5. We have now shown that protrudin directly associates with KIF5 and that protrudin and KIF5 synergistically promote protrusion formation in cells. Protrudin was found to link its associated proteins, such as Rab11, VAP-A and -B, Surf4, and RTN3, to KIF5, consistent with our observation that inhibition of the interaction between protrudin and KIF5 resulted in the accumulation of protrudin, as well as of Rab11, VAP-A and -B, Surf4, and RTN3 in the soma of cultured neurons.

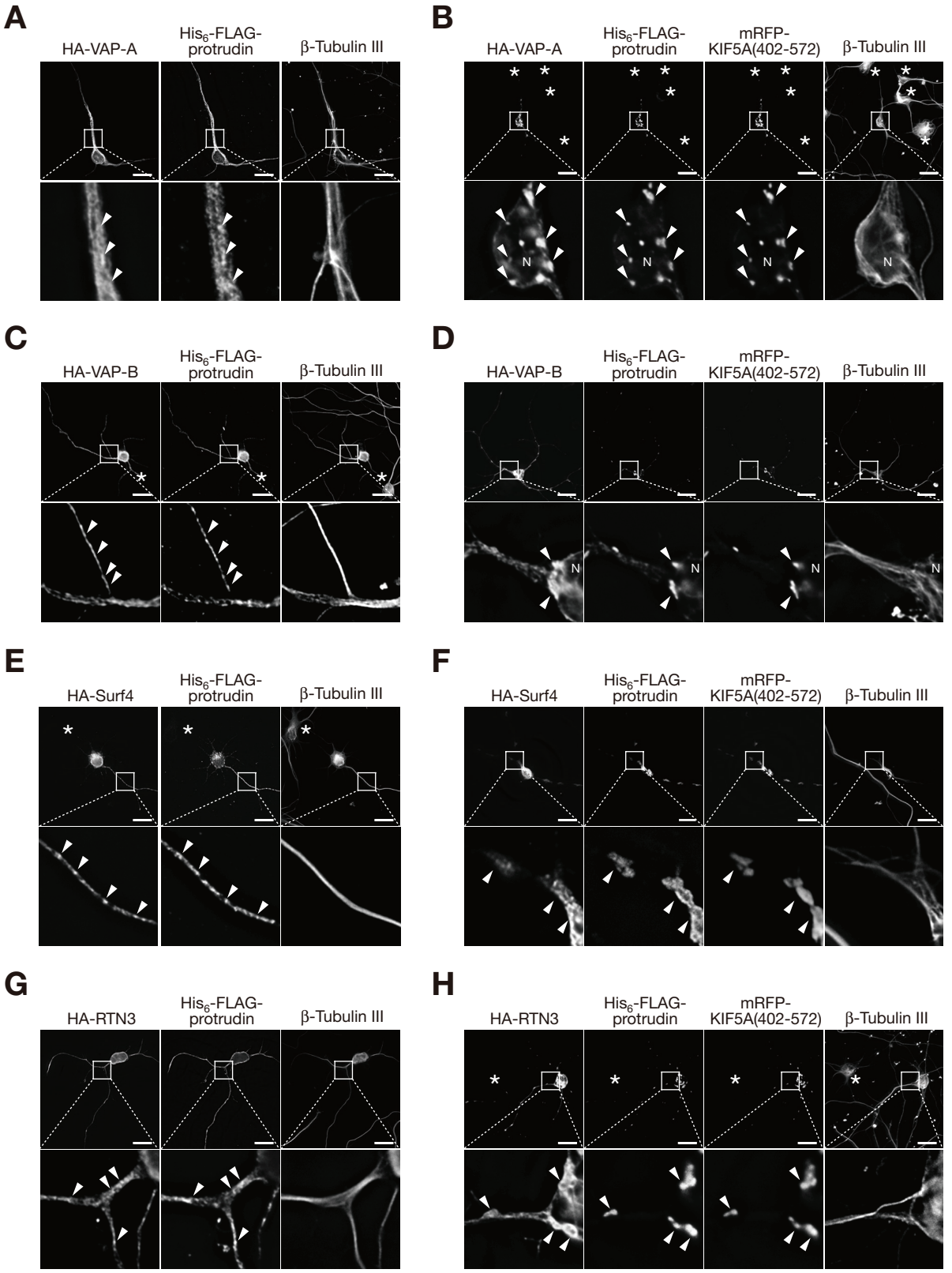

FIGURE 11: Protrudin accumulates with VAP-A or -B, Surf4, or RTN3 in the soma of neurons in response to inhibition of its association with KIF5. (A) Mouse cortical neurons expressing HA–VAP-A and His_6-FLAG–protrudin were subjected to immunofluorescence staining with anti-HA, anti-FLAG, and anti–β-tubulin III. Deconvoluted images are shown, with the boxed areas in the top panels presented at higher magnification in the bottom panels. Arrowheads indicate colocalization of HA–VAP-A and His_6-FLAG–protrudin in the neurite. Scale bars: 15 μm. (B) Mouse cortical neurons expressing HA–VAP-A, His_6-FLAG–protrudin, and mRFP-KIF5A(402–572) were subjected to immunofluorescence staining with anti-HA, anti-FLAG, and anti–β-tubulin III and were monitored for direct fluorescence of mRFP.

Protrudin-associated proteins are candidate cargoes for transport by protrudin and KIF5

The establishment and maintenance of neuronal polarity are fundamental to most aspects of neuronal function. Both protrudin and KIF5 have previously been shown to be important for neuronal activities (Ferreira *et al.*, 1992; Kimura *et al.*, 2005; Mannan *et al.*, 2006b; Shirane and Nakayama, 2006; Hirokawa *et al.*, 2009; Konishi and Setou, 2009). The identification of cargoes transported by the combination of protrudin and KIF5 is therefore likely to provide insight into the regulation of such activities.

VAP-A and -B were previously shown to interact with protrudin, and such interaction is required for neurite formation (Saita *et al.*, 2009). VAP-A interacts with a number of soluble *N*-ethylmaleimide-sensitive factor (NSF) attachment protein (SNAP) receptors and fusion-associated proteins, such as syntaxin 1A, Rbet1, Rsec22, αSNAP, and NSF (Weir *et al.*, 2001), suggestive of its function in neurons. VAP-33, *Aplysia* homologue of VAP-A and -B, was originally identified as a protein that binds to VAMP and was shown to contribute to the control of neurotransmitter release (Skehel *et al.*, 1995). VAP-33 is localized at the tight junction and intracellular vesicles for polarized vesicular transport in epithelial cells; it also localized in vesicles, including VAMP-2 and GLUT4, to regulate insulin-dependent translocation of GLUT4 to the plasma membrane in muscle or fat cells. Rab11 also regulates the trafficking of vesicles, including VAMP-2 and GLUT4. These observations suggest VAP-33 contributes to a variety of vesicular transport systems in association with Rab11 (Calhoun and Goldenring, 1997; Lapierre *et al.*, 1999, 2007; Lapierre, 2000; Foster *et al.*, 2000; Kessler *et al.*, 2000; Uhlig *et al.*, 2005). In addition, dVAP-33A of *Drosophila* regulates the division of boutons at presynaptic terminals during budding at neuromuscular junctions (Pennetta *et al.*, 2002; Chai *et al.*, 2008), and mutation of VAP-B has been associated with three forms of familial motor neuron disease: amyotrophic lateral sclerosis (ALS), atypical ALS, and late-onset spinal muscular atrophy (Nishimura *et al.*, 2004, 2005; Chen *et al.*, 2010). Collectively, these observations indicate the importance of VAP-A and -B in vesicular transport and neuronal function.

Surf4 is the mammalian orthologue of yeast Erv29p (Reeves and Fried, 1995), which serves as a cargo receptor, loading a specific subset of soluble cargo proteins, including glycosylated α-factor pheromone precursor and carboxypeptidase Y, into COPII vesicles departing from the endoplasmic reticulum (Belden and Barlowe, 2001). Given the extent of sequence similarity with Erv29p, Surf4 may perform a similar role in the transport of selective soluble cargoes in mammals, and protrudin and KIF5 might transport proteins that are loaded via Surf4.

RTN3 acts as an inhibitor of the β-site amyloid precursor protein (APP) cleaving enzyme 1 activity that cleaves APP to generate amyloid-β protein, which accumulates in the brain of individuals with Alzheimer's disease (He *et al.*, 2004; Murayama *et al.*, 2006). RTN3 aggregates in dystrophic neurites of the senile plaques in the brain of such individuals, and transgenic mice that express human RTN3 manifest formation of dystrophic neurites in the brain that correlates with impairment both of spatial learning and memory acquisition, as well as of synaptic plasticity (Hu *et al.*, 2007, 2009; Prior *et al.*, 2010). These observations suggest aggregation of RTN3 might contribute to the cognitive dysfunction associated with Alzheimer's disease by inducing neuritic dystrophy. Furthermore, an increase in the amount of RTN3 results in an imbalance in the axonal transport of this protein, which leads to its accumulation in swollen neurites, suggesting

Deconvoluted images are shown, with the boxed areas of the top panels presented at higher magnification in the bottom panels. The position of the nucleus is indicated by N. The asterisks indicate neurons not expressing HA–VAP-A, His_6-FLAG–protrudin, or mRFP-KIF5A(402–572), whereas the arrowheads indicate colocalization of HA–VAP-A, His_6-FLAG–protrudin, and mRFP-KIF5A(402–572) in the soma. Scale bars: 15 µm. (C) Mouse cortical neurons expressing HA–VAP-B and His_6-FLAG–protrudin were subjected to immunofluorescence staining with anti-HA, anti-FLAG, and anti–β-tubulin III. Deconvoluted images are shown, with the boxed areas in the top panels presented at higher magnification in the bottom panels. The asterisk indicates a neuron not expressing HA–VAP-B or His_6-FLAG–protrudin, whereas the arrowheads indicate colocalization of HA–VAP-B and His_6-FLAG–protrudin in the neurite. Scale bars: 15 µm. (D) Mouse cortical neurons expressing HA–VAP-B, His_6-FLAG–protrudin, and mRFP-KIF5A(402–572) were subjected to immunofluorescence staining with anti-HA, anti-FLAG, and anti–β-tubulin III and were monitored for direct fluorescence of mRFP. Deconvoluted images are shown, with the boxed areas of the top panels presented at higher magnification in the bottom panels. The position of the nucleus is indicated by N. The arrowheads indicate colocalization of HA–VAP-B, His_6-FLAG–protrudin, and mRFP-KIF5A(402–572) in the soma. Scale bars: 15 µm. (E) Mouse cortical neurons expressing HA-Surf4 and His_6-FLAG–protrudin were subjected to immunofluorescence staining with anti-HA, anti-FLAG, and anti–β-tubulin III. Deconvoluted images are shown, with the boxed areas in the top panels presented at higher magnification in the bottom panels. The asterisk indicates a neuron not expressing HA-Surf4 or His_6-FLAG–protrudin, whereas the arrowheads indicate colocalization of HA-Surf4 and His_6-FLAG–protrudin in the neurite. Scale bars: 15 µm. (F) Mouse cortical neurons expressing HA-Surf4, His_6-FLAG–protrudin, and mRFP-KIF5A(402–572) were subjected to immunofluorescence staining with anti-HA, anti-FLAG, and anti–β-tubulin III and were monitored for direct fluorescence of mRFP. Deconvoluted images are shown, with the boxed areas of the top panels presented at higher magnification in the bottom panels. The arrowheads indicate colocalization of HA-Surf4, His_6-FLAG–protrudin, and mRFP-KIF5A(402–572) in and near the soma. Scale bars: 15 µm. (G) Mouse cortical neurons expressing HA-RTN3 and His_6-FLAG–protrudin were subjected to immunofluorescence staining with anti-HA, anti-FLAG, and anti–β-tubulin III. Deconvoluted images are shown, with the boxed areas in the top panels presented at higher magnification in the bottom panels. Arrowheads indicate colocalization of HA-RTN3 and His_6-FLAG–protrudin in the neurite. Scale bars: 15 µm. (H) Mouse cortical neurons expressing HA-RTN3, His_6-FLAG–protrudin, and mRFP-KIF5A(402–572) were subjected to immunofluorescence staining with anti-HA, anti-FLAG, and anti–β-tubulin III and were monitored for direct fluorescence of mRFP. Deconvoluted images are shown, with the boxed areas of the top panels presented at higher magnification in the bottom panels. The asterisk indicates a neuron not expressing HA-RTN3, His_6-FLAG–protrudin, or mRFP-KIF5A(402–572), whereas the arrowheads indicate colocalization of HA-RTN3, His_6-FLAG–protrudin, and mRFP-KIF5A(402–572) in and near the soma. Scale bars: 15 µm.

the proper transport of RTN3 is important for the maintenance of neuronal function (Hu *et al.*, 2009).

Finally, Rab11 is also a candidate for a cargo molecule. Our previous (Shirane and Nakayama, 2006) and present studies indicate that protrudin interacts with both Rab11a and Rab11b through the Rab11-binding domain at its NH_2-terminus. Although Rab11 was not identified as a protrudin-associated protein by our LC–MS/MS analysis, this was possibly attributable to a low level of Rab11 expression in Neuro2A cells. In the brain, Rab11 is localized to the somatodendritic domain of neurons (Sheehan *et al.*, 1996) and is required for synaptic potentiation (Wang *et al.*, 2008). The formation of a GDP-Rab11–protrudin–KIF5 complex may activate KIF5 to bind to the microtubule track and transport protrudin, GDP-Rab11, and the associated membrane compartment to processes, given that KIF5 becomes activated for transport on cargo binding (Jiang and Sheetz, 1995; Coy *et al.*, 1999; Blasius *et al.*, 2007). We propose that the binding specificity of protrudin for the GDP-bound form of Rab11 might be important to maintain Rab11 in the inactive state during transport in neurons. After transport to the target site, GDP-Rab11 might be converted to GTP-Rab11 by the action of a guanine nucleotide exchange factor and unloaded from the protrudin–KIF5 complex to exert its function. Indeed, Rab11 was shown to play a pivotal role in α-amino-3-hydroxyl-5-methyl-4-isoxazole-propionate–sensitive glutamate receptor transport in association with myosin Vb at synapses (Wang *et al.*, 2008), suggesting that GDP-Rab11–KIF5 might be converted to GTP-Rab11–myosin Vb at synapses. Protrudin and KIF5 might therefore be required for the transport of Rab11 from the soma to the base of dendritic spines, where they may transfer it to myosin Vb, a motor protein that contributes to protein trafficking within the spine during long-term potentiation of synaptic strength. Similar regulation of the nucleotide state of Rab3 by its guanine nucleotide exchange factor was shown to be important for its axonal transport by kinesin family proteins (Niwa *et al.*, 2008).

Role of protrudin and KIF5A in HSP

AD-HSP comprises a group of genetically heterogeneous neurodegenerative disorders characterized by progressive spasticity of the lower limbs that is associated with retrograde degeneration of axons in the corticospinal tracts (Reid, 1997; Deluca *et al.*, 2004). To date, 45 spastic paraplegia (SPG) loci and 20 causative genes for AD-HSP, including those encoding ZFYVE27 (a synonym of human protrudin, SPG33) and KIF5A, have been identified (Reid *et al.*, 2002; Mannan *et al.*, 2006b). Mutations in KIF5A were recently identified in as many as 10% of cases of complicated HSP in individuals of European descent (Goizet *et al.*, 2009). In contrast, a point mutation in *ZFYVE27* has been described as the cause of pure HSP in a single German family (Mannan *et al.*, 2006b), although this mutation was recently detected in unaffected individuals (Martignoni *et al.*, 2008). It is possible that the pathogenic effects of this mutation differ among ethnic groups, especially given the clinical and genetic heterogeneity of, and presumed role of environmental factors in, HSP (Mannan, 2008). In the present study, we have demonstrated the molecular interaction of protrudin with KIF5, as well as the functional relation between these two proteins. We propose that protrudin and KIF5 constitute a system for the regulation of vesicular transport in neurons, and that dysfunction of this system might result in neurodegenerative disease. Protrudin also associates with spastin, the most commonly mutated protein in AD-HSP, which regulates the morphology of the endoplasmic reticulum together with atlastin-1, another commonly mutated protein in AD-HSP that associates with RTN3 (Mannan *et al.*, 2006b; Salinas *et al.*, 2007, 2008; Hu *et al.*, 2009; Park *et al.*, 2010). Furthermore, spastin associates with the RTN3-related protein RTN1 (Mannan *et al.*, 2006a). Together, these observations suggest that protrudin, through its complex relations with these various proteins, plays a key role in the maintenance of neuronal function. Further molecular analysis of protrudin and other AD-HSP–associated proteins, including KIF5A, may provide insight into the pathogenesis of this group of neurological disorders.

MATERIALS AND METHODS

Construction of expression plasmids

Mouse cDNAs encoding protrudin, KIF5A, KIF5B, KIF5C, KIF1Bα, and Surf4, as well as human cDNAs encoding KIF11, RTN3 (GenBank accession number NM_006054.2), and Rab11a (GenBank accession number NM_004663.4) were generated by PCR with PrimeSTAR HS DNA polymerase (Takara, Shiga, Japan) from cDNA preparations of Neuro2A cells or HEK293T cells. The cDNAs encoding mutants of these proteins were also generated by PCR. The cDNA encoding mouse protrudin (GenBank accession number NM_177319.3) was subcloned into the pmRFP-N3 or pmCherry-N3 vectors, which were generated from pEGFP-N3 (Clontech, Palo Alto, CA) by replacement of the EGFP sequence with the mRFP or mCherry sequences, respectively. The cDNA encoding mouse protrudin tagged at its NH_2-terminus with His_6-FLAG was subcloned into pcDNA3 (Invitrogen, Carlsbad, CA) or pMX-puro vectors (kindly provided by T. Kitamura). The cDNAs encoding wild-type or ΔCC mutant (Δ324–344) forms of mouse protrudin were subcloned into pcDNA3EF, which was generated from pcDNA3 by replacement of the cytomegalovirus promoter with the human elongation factor-1α gene promoter. The cDNAs encoding wild-type or T93N mutant forms of mouse KIF5A were subcloned into pEGFP-N1 or pEGFP-N3 (Clontech). The cDNAs encoding wild-type mouse KIF5A or various deletion mutants thereof (1–401, 402–1027 [headless], 402–807, 808–1027, 402–668, 669–807, 402–572, 573–807, or Δ402–572), a mutant form of mouse KIF5B (402–963 [headless]), a mutant form of mouse KIF5C (402–956 [headless]), a mutant form of mouse KIF1Bα (1375–3483 [headless]), human Rab11a, mouse Surf4, human RTN3, or EGFP were subcloned into pEF-BOS-2×HA (kindly provided by S. Nagata, Kyoto University, Japan). The cDNA encoding mouse Surf4 was subcloned into pEF-BOS-2×Myc (kindly provided by S. Nagata). The cDNA encoding mouse KIF5A(402–572) was subcloned into pmRFP-C1, which was generated from pEGFP-C1 (Clontech) by replacement of the EGFP sequence with the mRFP sequence. The cDNAs encoding wild-type or T93N mutant forms of mouse KIF5A were also subcloned into pcDNA3.1/Myc-His_6 (Invitrogen). The cDNA encoding human KIF11 tagged at its NH_2-terminus with the Myc epitope, as well as EGFP cDNA, were subcloned into pcDNA3. The cDNA encoding a mutant form of mouse KIF5A (1–572 [N]) tagged at its COOH-terminus with FLAG was subcloned into pcDNA3. The cDNAs encoding mutant forms of mouse KIF5A (1–401, 402–572, or 573–1027), wild-type or mutant (125–196) forms of human VAP-B, or human RTN3 were subcloned into pGEX-6P-1 (GE Healthcare, Little Chalfont, United Kingdom). Construction of vectors encoding human protrudin, Rab11b (GenBank accession number NM_004218.3) or Rab5b (Shirane and Nakayama, 2006) and those encoding human VAP-A or VAP-B (Saita *et al.*, 2009) was described previously. The cDNAs encoding mutant forms of human protrudin (1–206, 207–409, 247–409, 274–409, 318–409, 339–409, 207–361, 247–361, 274–361, Δ274–361, Δ318–338 [ΔCC], or 1–352 [ΔFYVE]) were subcloned into p3×FLAG-CMV-7.1 (Sigma, St. Louis, MO). The cDNA encoding human protrudin was also subcloned to pFastBac HT (Invitrogen).

Antibodies

Antibodies to protrudin were generated as described previously (Shirane and Nakayama, 2006). Anti-KIF5 (H2) was obtained from Chemicon (Temecula, CA); anti-Rab11(pan), anti-GM130, and anti-HSP90 were from BD Biosciences (San Jose, CA); anti-FLAG (M2 and polyclonal), anti-Myc (9E10), VAP-B (polyclonal), and anti–β-tubulin III were from Sigma; anti-HA (HA.11, used to detect HA-tagged proteins by default) were from Covance (Princeton, NJ); anti-His_6, anti-GST, and anti-GFP were from MBL (Nagoya, Japan); anti-Rab11a and anti-Rab11b were from Cell Signaling Technology (Danvers, MA); normal mouse immunoglobulin G (SC-2025) and anti-HA (Y-11) were from Santa Cruz Biotechnology (Santa Cruz, CA); Alexa Fluor 350–, 488–, 546–, or 633–conjugated goat antibodies to mouse or rabbit immunoglobulin G were from Molecular Probes (Eugene, OR).

Cell culture, transfection, and retroviral infection

Neuro2A, HEK293T, HeLa, Plat-E, and SHSY5Y cells were cultured under a humidified atmosphere of 5% CO_2 at 37°C in DMEM (Invitrogen) supplemented with 10% fetal bovine serum (FBS; Invitrogen). The culture medium for Plat-E cells was also supplemented with blasticidin. PC12 cells in RPMI-1640 medium (Sigma) supplemented with 10% FBS were cultured in six-well plates coated with poly-L-lysine (Sigma) for 2 d before exposure to mouse submaxillary gland nerve growth factor (50 ng/ml; Chemicon) in RPMI-1640 supplemented with 1% FBS. Neurons were isolated from the cerebral cortex of C57BL/6J mouse embryos at embryonic day 17 with the use of Nerve-Cell Culture System/Dissociation Solutions (Sumitomo Bakelite, Tokyo, Japan) and were cultured in Neuron culture medium (Sumitomo Bakelite) at a density of 8×10^4 cells per well in 24-well plates coated with poly-L-lysine. Mouse primary neurons were transfected with the use of Lipofectamine LTX and PLUS reagents (Invitrogen), PC12 cells were transfected with the use of an Amaxa Nucleofector instrument (program U-29) and Amaxa Nucleofector Kit V (Lonza, Cologne, Germany), and other cell types were transfected with the use of the FuGENE 6 or Fugene HD reagents (Roche, Mannheim, Germany). For retroviral infection, Plat-E cells were transiently transfected with pMX-puro–based vectors and then cultured for 48 h. The retroviruses in the resulting culture supernatants were used to infect Neuro2A cells, and the cells were then subjected to selection with puromycin.

Preparation of protein complexes by dual-affinity purification

Neuro2A cells (5×10^7) stably expressing His_6-FLAG–tagged mouse protrudin as a result of retroviral infection were disrupted with a Dounce homogenizer (type A pestle), the homogenate was centrifuged at $500 \times g$ for 5 min at 4°C to remove nuclei and nondisrupted cells, and the resulting supernatant was centrifuged at $100,000 \times g$ for 15 min at 4°C to isolate a membrane fraction (pellet). This pellet was solubilized with 1.6 ml of a lysis buffer (40 mM HEPES-NaOH, pH 7.5, 150 mM NaCl, 10% glycerol, 0.5% Triton X-100, 1 mM Na_3VO_4, 25 mM NaF, aprotinin [10 μg/ml], leupeptin [10 μg/ml], 1 mM phenylmethylsulfonyl fluoride [PMSF]), and the insoluble material was removed by centrifugation at $100,000 \times g$ for 1 h at 4°C. The protein concentration of the resulting supernatant was determined with the Bradford assay (Bio-Rad, Richmond, CA), and this soluble membrane fraction was then incubated with rotation for 45 min at 4°C with 40 μl of anti-FLAG (M2)–agarose affinity gel (Sigma) per milligram of protein. The beads were washed three times with lysis buffer, after which protein complexes were eluted for several minutes at 4°C with 800 μl of lysis buffer containing the FLAG peptide (Sigma) at 0.25 mg/ml. For the second affinity-purification step, nickel-nitrilotriacetic acid (Ni-NTA) agarose (ProBond resin, Invitrogen) was added to the eluate at one-half the volume of anti-FLAG (M2)–agarose used in the first step, and the mixture was incubated with rotation for 45 min at 4°C. The beads were washed three times with lysis buffer, and protein complexes were eluted for several minutes at 4°C with lysis buffer containing 300 mM imidazole.

Protein identification by LC–MS/MS analysis

The affinity-purified protein complexes were concentrated by precipitation with chloroform-methanol, fractionated by SDS–PAGE, and stained with silver. The stained gel was sliced into 10 equal pieces per lane, and the proteins therein were subjected to in-gel digestion with trypsin. The resulting peptides were dried, dissolved in a mixture of 0.1% trifluoroacetic acid and 2% acetonitrile, and then applied to a nanoflow LC system (Paradigm MS4; Michrom BioResources, Auburn, CA) equipped with an L-column (C_{18}, 0.15×50 mm, particle size of 3 μm; CERI, Tokyo, Japan). The peptides were fractionated with a linear gradient of solvent A (2% acetonitrile and 0.1% formic acid in water) and solvent B (90% acetonitrile and 0.1% formic acid in water), with 0–45% solvent B over 20 min, 45–95% over 5 min, and 95–5% over 1 min at a flow rate of 1 μl/min. Eluted peptides were sprayed directly into a Finnigan LTQ mass spectrometer (Thermo Fisher Scientific, San Jose, CA). MS and MS/MS spectra were obtained automatically in a data-dependent scan mode with a dynamic exclusion option. All MS/MS spectra were compared with protein sequences in the International Protein Index (IPI; European Bioinformatics Institute, Hinxton, United Kingdom) mouse version 3.44 with the use of the MASCOT algorithm. Trypsin was selected as the enzyme used, the allowed number of missed cleavages was set at one, and carbamidomethylation of cysteine was selected as a fixed modification. Oxidized methionine and NH_2-terminal pyroglutaminate were searched as variable modifications. Tolerance of MS/MS ions was 0.8 Da. Assigned high-scoring peptide sequences (MASCOT score of ≥45) were considered for correct identification. If the MASCOT score was <45, the criteria for match acceptance included the following: 1) peptide sequence length of ≥5, 2) a MASCOT score for individual peptides of ≥35, 3) at least three blocks of three successive matches or a block of six successive matches for y or b ions, and 4) a delta score of ≥12. Identified peptides from independent experiments were integrated and regrouped by IPI accession number.

Identification, semiquantitation, and categorization of protrudin-associated proteins

Proteins reproducibly detected in all three independent experiments with Neuro2A cells expressing protrudin as the bait, but not at all with mock cells, were considered protrudin-associated proteins. Semiquantitative estimation of protein abundance was based on IF (Matsumoto *et al.*, 2009), which is the number of identified peptides normalized by the number of peptides theoretically detectable with our instrument settings (molecular mass of 900–4000 Da). In this study, IF was normalized by the sum of the IFs for all the identified proteins in each experiment and then multiplied by 100 (normalized IF). The averages of normalized IF values for three independent experiments were ranked. Functional categorization of identified proteins was performed with the PANTHER classification system (www.pantherdb.org).

Immunoprecipitation and immunoblot analysis

Whole mouse brain was homogenized by 15 strokes (900 rpm) with a Potter homogenizer in a solution containing 20 mM HEPES-NaOH

(pH 7.6), 0.25 M sucrose, 1 mM EDTA, 1 mM Na_3VO_4, 25 mM NaF, aprotinin (10 μg/ml), leupeptin (10 μg/ml), and 1 mM PMSF. The homogenate was centrifuged twice at 1000 × *g* for 10 min at 4°C, and the second supernatant was centrifuged at 100,000 × *g* for 1 h at 4°C. The crude microsomal pellet was resuspended in the lysis buffer described above, incubated for 1 h at 4°C, and then centrifuged again at 100,000 × *g* for 1 h at 4°C to remove insoluble material. The resulting supernatant was then subjected to immunoprecipitation (IP) for 2 h at 4°C with anti-protrudin (or normal rabbit serum) and protein G–Sepharose 4 Fast Flow (Amersham Biosciences, Uppsala, Sweden). The immunoprecipitates were washed three times with lysis buffer and were then subjected to IB, as described previously (Shirane and Nakayama, 2006). The images were scanned with LAS-1000 (Fujifilm, Tokyo, Japan) or LAS-4000 (GE Healthcare) instruments. For analysis of transfected HEK293T or HeLa cells, the cells were cultured for 1 d after transfection and then lysed by incubation for 10 min at 4°C with lysis buffer. The lysates were centrifuged at 20,400 × *g* for 10 min at 4°C, and equal amounts of protein from the resulting supernatants were subjected directly to IB or to IP for 45 min at 4°C with anti-FLAG (M2)–agarose affinity gel, which was followed by IB.

In vitro binding assay

Recombinant GST-tagged KIF5A (1–401, 402–572, or 573–1027), VAP-B (wild-type or 125–196), and RTN3 were expressed in and purified from *Escherichia coli*. The BL21(DE3)pLysS bacterial cells were transformed with the pGEX-6P-1–based vectors, or with pGEX-6P-1 as a negative control. Overnight cultures of the transformed cells were diluted 1:20 with 2× YT medium (Gibco, Paisley, United Kingdom) containing ampicillin, grown at 37°C for 2 h, and then exposed to 0.2 mM isopropyl-β-D-thiogalactopyranoside for 12 h at 16°C. Expressed proteins were purified from the soluble fraction of cell lysates with glutathione–Sepharose 4B beads (Amersham Biosciences). The purified GST-tagged KIF5A and RTN3 proteins (or GST as the negative control) were eluted from the beads with reduced glutathione. The purified GST–VAP-B proteins were used without elution from the beads. Recombinant His_6-protrudin was expressed in and purified from *Spodoptera frugiperda* (cell line Sf21) insect cells with the use of the Bac-to-Bac system (Invitrogen). Recombinant virus was produced with pFastBac HT-protrudin. Sf21 cells were infected with recombinant virus for 72 h, and the expressed protein was purified from the soluble fraction of cell lysates with Ni-NTA agarose and subsequently eluted with 300 mM imidazole. GST-KIF5A, GST-RTN3, or GST proteins were incubated with glutathione–Sepharose 4B beads in lysis buffer described above for 1 h at 4°C with rotation, and the beads were then washed three times with lysis buffer. His_6-protrudin was incubated with the beads containing bound GST fusion proteins or GST for 1 h at 4°C with rotation, after which the beads were washed three times with lysis buffer, and the bound proteins were subjected to IB or to silver staining (Daiichi Kagaku, Tokyo, Japan).

Immunostaining

HeLa and PC12 cells, as well as neurons cultured on glass coverslips, were prepared for immunostaining. HeLa and PC12 cells were fixed for 10 min at room temperature with 3.7% formaldehyde in phosphate-buffered saline (PBS). In some experiments, the cells were exposed to 0.1% Triton X-100 for 10 s before fixation. Neurons were fixed for 15 min with 3.7% formaldehyde and 4% sucrose in PBS and were permeabilized with 0.1% Triton X-100 in PBS for 10 min at room temperature. HeLa and PC12 cells were then incubated consecutively with primary antibodies and Alexa Fluor 350–, 488–, 546–, or 633–labeled goat secondary antibodies in PBS containing 0.5% bovine serum albumin (BSA) and 0.1% saponin, and neurons were exposed to the antibodies in PBS containing 1.0% BSA. The cells were also stained with Hoechst 33258 (Wako, Tokyo, Japan) in some experiments. Cells were covered with a drop of GEL/MOUNT (Biomeda, Hayward, CA) for observation.

Imaging

Cells were observed with a DeltaVision RT system (Applied Precision, Issaquah, WA) that was attached to an Olympus IX-71 inverted microscope fitted with an IX-HLSH100 CCD camera and 20×/0.75 UPlanSApo, 40×/1.35 UApo/340, 60×/1.42 PlanApo N, and 100×/1.40 UplanSApo objectives (Olympus, Tokyo, Japan). For observation of cellular morphology, images were acquired with the 20× objective lens without deconvolution. For observation of the intracellular localization of proteins, images were collected as stacks with 0.2-μm increments in the *z*-axis with the 100× objective lens, and the stacked images were deconvoluted with a constrained iterative algorithm provided with SoftWoRx (Applied Precision). For time-lapse imaging, cells were maintained at 37°C under 5% CO_2 in a chamber. Images were obtained at 8-min intervals from 16 to 24 h after transfection.

Quantitation of protrusion formation

For evaluation of the effect of protein overexpression or depletion on the formation of cell protrusions, 40 nonoverlapping images (each 1024 × 1024) were collected with the 20× objective lens from each sample of HeLa cells that had been cultured for 20 or 48 h after transfection and then fixed and immunostained. The cells with processes whose length was greater than the longest diameter of the nucleus were counted, and the ratio of the number of these cells to the total number of cells overexpressing protrudin or KIF5A (or EGFP) was determined.

RNAi

DNA fragments encoding stem loop–type shRNAs specific for human protrudin mRNA (5′-GCTGAGGTGAAGAGCTTCTTG-3′), human KIF5B mRNA (5′-GCAGTCAGGTCAAAGAATATG-3′), or EGFP mRNA (5′-GCTGACCCTGAAGTTCATC-3′) were synthesized, attached to the U6 promoter, and subcloned into the pBluescriptII SK(+) vector (Stratagene, LaJolla, CA). The vectors were introduced by transfection into HeLa cells, and the knockdown efficiency was assessed after 2 d by reverse transcription (RT) and real-time PCR analysis with cells expressing the EGFP shRNA as a control. Stealth siRNAs designed for human Rab11a (5′-AAACCAAUAAGGCACCUACAGCUCC-3′) or Rab11b (5′-UACGUUAGUGGAAUCCAAGGCUGAG-3′), or negative control duplexes (Invitrogen), were introduced into HeLa cells by reverse transfection with Lipofectamine RNAiMax (Invitrogen), and the knockdown efficiency was assessed after 2 d by RT and real-time PCR analysis and after 3 d by IB, with cells transfected with the negative control duplexes as a control.

RT-PCR

Total RNA (1 μg) isolated from cultured cells with the use of Isogen (Wako) was subjected to RT with a Quantitect kit (Qiagen, Hilden, Germany). The resulting cDNA was subjected to PCR with Taq polymerase (Takara) or to real-time PCR, as described previously (Yada *et al.*, 2004). The amount of each target mRNA was normalized by the corresponding amount of glyceraldehyde-3-phosphate dehydrogenase (GAPDH) mRNA. Primers for PCR were as follows (forward and reverse, respectively): 5′-ACACGAGAAGAGCACCAAGC-3′ and 5′-GACTGCTCATGTCGCTCGTA-3′ for human KIF5A; 5′-CACAACCTGCGCAAACTCT-3′ and 5′-TCCGGTGTCATCAGAATCAA-3′ for

human KIF5B; 5′-CAGCATCTGGAGATGGAGCTA-3′ and 5′-TTCATCCTCAGGCACAGCTT-3′ for human KIF5C; and 5′-ACCACAGTCCATGCCATCAC-3′ and 5′-TCCACCACCCTGTTGCTGTA-3′ for human GAPDH. Primers for real-time PCR were as follows: 5′-GTCCTCCACCACCAGATGTT-3′ and 5′-TGAGGTCCTGGGAAGAGAGA-3′ for human protrudin; 5′-CACAACCTGCGCAAACTCT-3′ and 5′-TCCGGTGTCATCAGAATCAA-3′ for human KIF5B; and 5′-ACCACAGTCCATGCCATCAC-3′ and 5′-TCCACCACCCTGTTGCTGTA-3′ for human GAPDH.

Statistical analysis

Quantitative data are presented as means ± SD and were analyzed by Student's *t* test or by one-way or two-way ANOVA, which was followed by multiple comparisons with the Tukey-Kramer test. A p value of <0.05 was considered statistically significant.

ACKNOWLEDGMENTS

We thank S. Nagata and T. Kitamura for vectors; N. Nishimura, Y. Yoshimura, A. Hamasaki, and A. Kanebayashi for technical assistance; K. Oyamada and T. Takami for programming and system operation; S. Saita, E. Susaki, K. Oshikawa, and T. Moroishi for discussion and construction of expression plasmids; A. Ohta for help in preparation of the manuscript; and M. Oda, E. Koba, K. Fukidome, and M. Otsu for maintenance of equipment and other technical assistance.

REFERENCES

Belden WJ, Barlowe C (2001). Role of Erv29p in collecting soluble secretory proteins into ER-derived transport vesicles. Science 294, 1528–1531.

Blasius TL, Cai D, Jih GT, Toret CP, Verhey KJ (2007). Two binding partners cooperate to activate the molecular motor Kinesin-1. J Cell Biol 176, 11–17.

Cai D, Hoppe AD, Swanson JA, Verhey KJ (2007). Kinesin-1 structural organization and conformational changes revealed by FRET stoichiometry in live cells. J Cell Biol 176, 51–63.

Calhoun BC, Goldenring JR (1997). Two Rab proteins, vesicle-associated membrane protein 2 (VAMP-2) and secretory carrier membrane proteins (SCAMPs), are present on immunoisolated parietal cell tubulovesicles. Biochem J 325, 559–564.

Chai A, Withers J, Koh YH, Parry K, Bao H, Zhang B, Budnik V, Pennetta G (2008). *hVAPB*, the causative gene of a heterogeneous group of motor neuron diseases in humans, is functionally interchangeable with its *Drosophila* homologue *DVAP-33A* at the neuromuscular junction. Hum Mol Genet 17, 266–280.

Chen HJ, Anagnostou G, Chai A, Withers J, Morris A, Adhikaree J, Pennetta G, de Belleroche JS (2010). Characterisation of the properties of a novel mutation in VAPB in familial ALS. J Biol Chem 285, 40266–40281.

Cho KI, Cai Y, Yi H, Yeh A, Aslanukov A, Ferreira PA (2007). Association of the kinesin-binding domain of RanBP2 to KIF5B and KIF5C determines mitochondria localization and function. Traffic 8, 1722–1735.

Coy DL, Hancock WO, Wagenbach M, Howard J (1999). Kinesin's tail domain is an inhibitory regulator of the motor domain. Nat Cell Biol 1, 288–292.

Deluca GC, Ebers GC, Esiri MM (2004). The extent of axonal loss in the long tracts in hereditary spastic paraplegia. Neuropathol Appl Neurobiol 30, 576–584.

Ferreira A, Niclas J, Vale RD, Banker G, Kosik KS (1992). Suppression of kinesin expression in cultured hippocampal neurons using antisense oligonucleotides. J Cell Biol 117, 595–606.

Foster LJ, Weir ML, Lim DY, Liu Z, Trimble WS, Klip A (2000). A functional role for VAP-33 in insulin-stimulated GLUT4 traffic. Traffic 1, 512–521.

Futerman AH, Banker GA (1996). The economics of neurite outgrowth–the addition of new membrane to growing axons. Trends Neurosci 19, 144–149.

Glater EE, Megeath LJ, Stowers RS, Schwarz TL (2006). Axonal transport of mitochondria requires milton to recruit kinesin heavy chain and is light chain independent. J Cell Biol 173, 545–557.

Goizet C *et al.* (2009). Complicated forms of autosomal dominant hereditary spastic paraplegia are frequent in SPG10. Hum Mutat 30, E376–E385.

Goldstein AY, Wang X, Schwarz TL (2008). Axonal transport and the delivery of pre-synaptic components. Curr Opin Neurobiol 18, 495–503.

Goldstein LS (2001). Kinesin molecular motors: transport pathways, receptors, and human disease. Proc Natl Acad Sci USA 98, 6999–7003.

Gyoeva FK, Sarkisov DV, Khodjakov AL, Minin AA (2004). The tetrameric molecule of conventional kinesin contains identical light chains. Biochemistry 43, 13525–13531.

He W, Lu Y, Qahwash I, Hu XY, Chang A, Yan R (2004). Reticulon family members modulate BACE1 activity and amyloid-β peptide generation. Nat Med 10, 959–965.

Hirokawa N, Noda Y (2008). Intracellular transport and kinesin superfamily proteins, KIFs: structure, function, and dynamics. Physiol Rev 88, 1089–1118.

Hirokawa N, Noda Y, Tanaka Y, Niwa S (2009). Kinesin superfamily motor proteins and intracellular transport. Nat Rev Mol Cell Biol 10, 682–696.

Hu J, Shibata Y, Zhu PP, Voss C, Rismanchi N, Prinz WA, Rapoport TA, Blackstone C (2009). A class of dynamin-like GTPases involved in the generation of the tubular ER network. Cell 138, 549–561.

Hu X, Shi Q, Zhou X, He W, Yi H, Yin X, Gearing M, Levey A, Yan R (2007). Transgenic mice overexpressing reticulon 3 develop neuritic abnormalities. EMBO J 26, 2755–2767.

Jiang MY, Sheetz MP (1995). Cargo-activated ATPase activity of kinesin. Biophys J 68, 283S–284S, discussion 285S.

Kessler A, Tomas E, Immler D, Meyer HE, Zorzano A, Eckel J (2000). Rab11 is associated with GLUT4-containing vesicles and redistributes in response to insulin. Diabetologia 43, 1518–1527.

Kimura T, Watanabe H, Iwamatsu A, Kaibuchi K (2005). Tubulin and CRMP-2 complex is transported via Kinesin-1. J Neurochem 93, 1371–1382.

Konishi Y, Setou M (2009). Tubulin tyrosination navigates the kinesin-1 motor domain to axons. Nat Neurosci 12, 559–567.

Lapierre LA (2000). The molecular structure of the tight junction. Adv Drug Deliv Rev 41, 255–264.

Lapierre LA, Avant KM, Caldwell CM, Ham AJ, Hill S, Williams JA, Smolka AJ, Goldenring JR (2007). Characterization of immunoisolated human gastric parietal cells tubulovesicles: identification of regulators of apical recycling. Am J Physiol Gastrointest Liver Physiol 292, G1249–1262.

Lapierre LA, Tuma PL, Navarre J, Goldenring JR, Anderson JM (1999). VAP-33 localizes to both an intracellular vesicle population and with occludin at the tight junction. J Cell Sci 112, 3723–3732.

Mannan AU (2008). The role of ZFYVE27/protrudin in hereditary spastic paraplegia—response to Martignoni et al. Am J Hum Genet 83, 128–130.

Mannan AU, Boehm J, Sauter SM, Rauber A, Byrne PC, Neesen J, Engel W (2006a). Spastin, the most commonly mutated protein in hereditary spastic paraplegia interacts with Reticulon 1 an endoplasmic reticulum protein. Neurogenetics 7, 93–103.

Mannan AU, Krawen P, Sauter SM, Boehm J, Chronowska A, Paulus W, Neesen J, Engel W (2006b). ZFYVE27 (SPG33), a novel spastin-binding protein, is mutated in hereditary spastic paraplegia. Am J Hum Genet 79, 351–357.

Martignoni M, Riano E, Rugarli EI (2008). The role of ZFYVE27/protrudin in hereditary spastic paraplegia. Am J Hum Genet 83, 127–128.

Matsumoto M, Oyamada K, Takahashi H, Sato T, Hatakeyama S, Nakayama KI (2009). Large-scale proteomic analysis of tyrosine-phosphorylation induced by T-cell receptor or B-cell receptor activation reveals new signaling pathways. Proteomics 9, 3549–3563.

Murayama KS, Kametani F, Saito S, Kume H, Akiyama H, Araki W (2006). Reticulons RTN3 and RTN4-B/C interact with BACE1 and inhibit its ability to produce amyloid β-protein. Eur J Neurosci 24, 1237–1244.

Nakata T, Hirokawa N (1995). Point mutation of adenosine triphosphate-binding motif generated rigor kinesin that selectively blocks anterograde lysosome membrane transport. J Cell Biol 131, 1039–1053.

Nishimura AL, Al-Chalabi A, Zatz M (2005). A common founder for amyotrophic lateral sclerosis type 8 (ALS8) in the Brazilian population. Hum Genet 118, 499–500.

Nishimura AL *et al.* (2004). A mutation in the vesicle-trafficking protein VAPB causes late-onset spinal muscular atrophy and amyotrophic lateral sclerosis. Am J Hum Genet 75, 822–831.

Niwa S, Tanaka Y, Hirokawa N (2008). KIF1Bβ- and KIF1A-mediated axonal transport of presynaptic regulator Rab3 occurs in a GTP-dependent manner through DENN/MADD. Nat Cell Biol 10, 1269–1279.

Park SH, Zhu PP, Parker RL, Blackstone C (2010). Hereditary spastic paraplegia proteins REEP1, spastin, and atlastin-1 coordinate microtubule interactions with the tubular ER network. J Clin Invest 120, 1097–1110.

Pennetta G, Hiesinger PR, Fabian-Fine R, Meinertzhagen IA, Bellen HJ (2002). *Drosophila* VAP-33A directs bouton formation at neuromuscular junctions in a dosage-dependent manner. Neuron 35, 291–306.
Prior M, Shi Q, Hu X, He W, Levey A, Yan R (2010). RTN/Nogo in forming Alzheimer's neuritic plaques. Neurosci Biobehav Rev 34, 1201–1206.
Reeves JE, Fried M (1995). The surf-4 gene encodes a novel 30 kDa integral membrane protein. Mol Membr Biol 12, 201–208.
Reid E (1997). Pure hereditary spastic paraplegia. J Med Genet 34, 499–503.
Reid E *et al*. (2002). A kinesin heavy chain (KIF5A) mutation in hereditary spastic paraplegia (SPG10). Am J Hum Genet 71, 1189–1194.
Saita S, Shirane M, Natume T, Iemura S, Nakayama KI (2009). Promotion of neurite extension by protrudin requires its interaction with vesicle-associated membrane protein-associated protein. J Biol Chem 284, 13766–13777.
Salinas S, Carazo-Salas RE, Proukakis C, Schiavo G, Warner TT (2007). Spastin and microtubules: functions in health and disease. J Neurosci Res 85, 2778–2782.
Salinas S, Proukakis C, Crosby A, Warner TT (2008). Hereditary spastic paraplegia: clinical features and pathogenetic mechanisms. Lancet Neurol 7, 1127–1138.
Setou M, Seog DH, Tanaka Y, Kanai Y, Takei Y, Kawagishi M, Hirokawa N (2002). Glutamate-receptor-interacting protein GRIP1 directly steers kinesin to dendrites. Nature 417, 83–87.
Sheehan D, Ray GS, Calhoun BC, Goldenring JR (1996). A somatodendritic distribution of Rab11 in rabbit brain neurons. NeuroReport 7, 1297–1300.
Shirane M, Nakayama KI (2006). Protrudin induces neurite formation by directional membrane trafficking. Science 314, 818–821.
Skehel PA, Martin KC, Kandel ER, Bartsch D (1995). A VAMP-binding protein from Aplysia required for neurotransmitter release. Science 269, 1580–1583.
Stenmark H (2009). Rab GTPases as coordinators of vesicle traffic. Nat Rev Mol Cell Biol 10, 513–525.
Su Q, Cai Q, Gerwin C, Smith CL, Sheng ZH (2004). Syntabulin is a microtubule-associated protein implicated in syntaxin transport in neurons. Nat Cell Biol 6, 941–953.
Tang BL (2001). Protein trafficking mechanisms associated with neurite outgrowth and polarized sorting in neurons. J Neurochem 79, 923–930.
Uhlig M, Passlack W, Eckel J (2005). Functional role of Rab11 in GLUT4 trafficking in cardiomyocytes. Mol Cell Endocrinol 235, 1–9.
Ullrich O, Stenmark H, Alexandrov K, Huber LA, Kaibuchi K, Sasaki T, Takai Y, Zerial M (1993). Rab GDP dissociation inhibitor as a general regulator for the membrane association of rab proteins. J Biol Chem 268, 18143–18150.
Wang Z *et al*. (2008). Myosin Vb mobilizes recycling endosomes and AMPA receptors for postsynaptic plasticity. Cell 135, 535–548.
Weir ML, Xie H, Klip A, Trimble WS (2001). VAP-A binds promiscuously to both v- and tSNAREs. Biochem Biophys Res Commun 286, 616–621.
Yada M, Hatakeyama S, Kamura T, Nishiyama M, Tsunematsu R, Imaki H, Ishida N, Okumura F, Nakayama K, Nakayama KI (2004). Phosphorylation-dependent degradation of c-Myc is mediated by the F-box protein Fbw7. EMBO J 23, 2116–2125.
Yang JT, Laymon RA, Goldstein LS (1989). A three-domain structure of kinesin heavy chain revealed by DNA sequence and microtubule binding analyses. Cell 56, 879–889.